A comparative study of two SOFC based cogeneration systems fed by municipal solid waste by means of either the gasifier or digester

(Article begins on next page)

1 **A comparative study of two SOFC based cogeneration systems fed by municipal solid**

2 **waste by means of either the gasifier or digester**

3 M. Yari[1], A. S. Mehr[1,*], SMS Mahmoudi[1] and M. Santarelli[2]

4
5 1. Faculty of Mechanical Engineering. University of Tabriz, Tabriz, Iran
2. Department of Energy, Politecnico di Torino, C.so Duca degli Abruzzi 24, 10129, Turin, Italy
6

7 **Abstract**

8 Two new cogeneration systems (producing power and heating) based on solid oxide fuel cell

9 fed by either the syngas or biogas is proposed. The performance of systems is analyzed and

10 compared with each other from the thermodynamic and economic viewpoints. Applying the

11 conservation of mass and energy as well as the exergy and cost balance for each system

12 component and using the engineering equation solver software, the systems are modeled.

13 Through a parametric study, effect of some key variables such as the current density and the

14 stack temperature difference on the systems' performance is investigated. It is found that for

15 power generation, digester based solid oxide fuel cell shows better performance of first law

16 efficiency (40.14% vs 20.31%); however considering the combined power and heating system,

17 the difference becomes less (51.05% vs 58.75%). In addition, it is found that the digester based

18 SOFC is more cost-efficient and has 54% less unit product cost compared to that of the gasifier

19 based system. Results of exergy analysis reveal that the air heat exchangers and the gasifier are

20 the two major sources of irreversibility in the systems. Finally, a method of choosing the systems

21 based on the need and the cost is presented.

22 **Keywords:** *SOFC, Biogas, Syngas, Gasifier, Anaerobic Digester, Exergoeconomic, comparative study*

23 ***Corresponding author e-mail:** a.s.mehr@tabrizu.ac.ir (Ali Saberi Mehr)

24 Tel.: +98 41 33392487; fax: +98 41 33354153.

25

Nomenclature

AD	Anaerobic digester		*Subscript and abbreviations*	
AHX	Air heat exchanger		0	dead state
D-SOFC	Digester coupled SOFC		1,2,3,…	state points
G-SOFC	Gasifier coupled SOFC			
SOFC	Solid oxide fuel cell		*Greek Symbols*	
HRSG	Heat recovery steam generator		η_{th}	thermal efficiency
EES	Engineering Equation Solver			
FHX	Fuel heat exchanger		η_{II}	exergy efficiency
FuelB	Fuel blower		η_{I}	energy efficiency
AirB	Air blower		η_{is}	isentropic efficiency
P	pump			
K	equilibrium constant			
ΔG	Change in Gibbs function			
S	entropy			
h	enthalpy			
$\dot{W}$	Power			
$\dot{Q}$	Heating load			

26

27

28

1. Introduction

Since the world's energy consumption is forecast to rise remarkably during the next two decades, no one can deny the importance of renewable energy sources. In addition, continued demand for fossil fuels means the world will not be able to reduce greenhouse gases in the atmosphere. In this regard, implementing the power plants utilizing the renewable energy sources such as geothermal, solar, biofuel, biomass and so on, is supposed to be of governments' and researchers' interest.

Recent developments in solid oxide fuel cell (SOFC) technology have increased interest in the application toward electricity generation particularly the distributed one. In addition to the advantages of SOFC system over conventional power generation methods, heat from SOFC exhaust can be recovered for combined heat and power (CHP) operations to improve the overall system efficiency.

Undoubtedly, the hydrogen is the genuine fuel for the stack; however, considering its cost and availability, using the natural gas could be more viable, practical and economical in addition to the reforming process of the fuel. Nevertheless, feeding the SOFC with fuels such as biogas, biofuels, syngas and alcohols has become of great interest as they could be suitable alternatives for the natural gas. There are numerous solid waste gasification facilities operating or under construction around the world. Gasification has several advantages over traditional combustion processes for municipal solid waste (MSW) treatment. It takes place in a low oxygen environment that limits the formation of dioxins and of large quantities of SO_x and NO_x. Furthermore, it requires just a fraction of the stoichiometric amount of oxygen necessary for combustion (partial oxidation). As a result, the volume of process gas is low, requiring smaller and less expensive gas cleaning equipment. The lower gas volume also means higher partial

3

52   pressure of contaminants in the off-gas, which favors more complete adsorption and particulate

53   capture. Finally, gasification generates a fuel gas that can be integrated with combined cycle

54   turbines, reciprocating engines and, potentially, with fuel cells converting fuel energy to

55   electricity more efficiently than conventional steam boilers[1,2]. Renewability and less CO_2

56   emission are the greatest advantages of commonly used biomass fuels such as paper, wood,

57   waste straw, saw dust, paddy husk, MSW, etc. [3–6].Three processes are usually involved in

58   thermochemical conversion of biomass into usable fuels for power plants: combustion,

59   gasification and pyrolysis [7,8]. The gasification process proves to be an efficient technique as it

60   transforms biomass into easily usable fuels to be used for electricity generation [9–11]. There are

61   different types of gasifiers based on the types of moving fluid and solid inside[12]. From the

62   availability view point however, 75% percent of the gasifiers are downdraft, 20% is circulating

63   fluidized bed, 2.5% updraft and 2.5% the other kinds [13].

64   A 200kW SOFC combined heat and power system has been developed by Omosun et al. [14]

65   to evaluate the system efficiency and its cost analysis. Two different options were investigated;

66   one of them involved cold gas cleaning and the other used hot gas cleaning. The results revealed

67   that system efficiency for the hot process is higher than that for the cold process due to the better

68   heat management in the cleaning process and higher gasification temperature. Despite the capital

69   cost for the hot process is marginally higher, income earned from selling the extra heat produced

70   may justify the additional cost. Singh et al. [15] analyzed the carbon deposition in a solid oxide

71   fuel cell (SOFC) fueled by a biomass. It is reported that carbon deposition decreased to zero as

72   the operating conditions were varied to get a fuel mixture with higher water content (about 15%).

73   The conjunction of biomass gasification with solid oxide fuel cells is investigated by Athanasiou

74   et al. [16] and the results showed that the electrical efficiency of the integrated gasification-

4

75   SOFC-steam turbine is about 68% higher than that for the conventional gasification-steam

76   turbine system. A direct internal reforming-SOFC (IR-SOFC) operating with syngas was

77   modeled thermodynamically by Colpan et al [17]. The results showed that recirculation ratio

78   does not have a significant effect for low current density conditions. However, at higher current

79   densities, increasing the recirculation ratio decreases the output power and electrical efficiency

80   of the cell. Jang et al. [18] studied a direct power generation from waste coffee grounds

81   in a biomass fed fuel cell. Results show that biomass type has crucial effect on cell performance.

82   They used waste coffee ground (WCG) as biomass with the benefit of not needing any pre-

83   reformer in the system. It is reported that at cell operating temperature of $900^{o}C$ the system

84   shows maximum power density twice than that of the carbon black. Pieratti et al. [19]

85   investigated experimentally and theoretically the syngas suitability for solid oxide fuel cell

86   applications. Considering environmental aspects of biomass combustion, steam gasification is

87   used to produce syngas. Experimental data is used to generate and calibrate a 2D theoretical

88   equilibrium model. It is found that the thermodynamic approach is a simple engineering useful

89   tool to obtain reliable results of the gasification model. It is declared that considering the syngas

90   composition and energy content, the obtained syngas is a suitable fuel for fuel cells.

91   Nevertheless, the gas cleaning is still one of the main critical issues. In particular the tar and the

92   H_2S in the gas can rapidly decrease the life of the fuel cells. A new small cogeneration system

93   consisting of a fluidized bed gasifier, coupled to a SOFC and a micro gas turbine is proposed by

94   Di Carlo et al. [20]. Results disclosed that the best case occurs with a temperature of the cathode

95   gas of $800\ ^{o}C$ and moisture of 10%, in this case the fuel utilization could be set equal to 0.79 and

96   the electrical efficiency of the overall system is 48%. Focusing on the anode gas recycling,

97   Lorenzo and Fragiacomo [21] analyzed the performance of syngas fed SOFC power plant from

98   the viewpoint of thermodynamics. It is reported that there is an optimum value for anode gas

99   recycle ratio in which the thermal efficiency is maximized. An integrated SOFC and biomass

100   (wood) gasification system using air, enriched air, and steam as gasification agent is investigated

101   by Jia et al. [22]. It is found that when using air or oxygen-enriched air as gasification agent, the

102   gasifier reactor caused the greatest exergy destruction while for steam gasification power

103   systems the largest exergy destruction lies in air heat exchanger. Also, for the efficient CHP case

104   the exergy efficiency is calculated to be 36%. In another work, Jia et al. [23] studied the effects

105   of various parameters such as moisture content in biomass, equivalence ratio and mass flow rate

106   of dry biomass on the overall performance of SOFC based CHP system. It is reported that char in

107   the biomass tends to be converted with decreasing of moisture content and increasing of

108   equivalence ratio due to higher temperature in reduction zone of gasifier. Kartha et al. [24]

109   studied a small-scale biomass fuel cell/gas turbine power systems for rural areas. A downdraft

110   gasifier is used to produce syngas because it is reported to be commercialized and simple in

111   design which has very little amounts of tar (the excessive production of which needs a separate

112   reactor for tar removal and dissipates amounts of flue gas energy) and has simple method of gas

113   cleaning. Also, the efficiency of the studied SOFC-GT was found to be 43.4%. Federico

114   Ghirardo et al. [25] studied heat recovery options for fuel cells. It is found that about 181 kW of

115   heat can be recovered in an ORC to produce 35 kW of electricity. The overall efficiency

116   increases from 44% to 49% when the recovery system is used and the cost of energy drops from

117   25 c$/kWh (isolated SOFC system) to 22 c$/kWh.

118   Even though continued progress has been made with other alternative treatment technologies

119   (gasification, pyrolysis, plasma, biological drying, etc.), these technologies have by far not seen

120   the same widespread implementation that anaerobic digestion has been able to achieve. In

121   Europe alone, 244 installations dealing with the organic fraction of municipal solid waste as a

122   significant portion of the feedstock have been constructed or are permitted to be constructed.

123   Feeding SOFCs by biogas is investigated by researchers in the recent years. The performance of

124   biogas-fed solid oxide fuel cell system utilizing different reforming agents (steam, air and

125   combined air/steam) was investigated by Piroonlerkgul et al. [26]. It is observed that for the

126   steam-fed SOFC, there is an optimal amount of steam which provides a maximum power

127   density. However, for the air-fed SOFC system, the power density always decreases with the

128   increase of amount of air due to the dilution effect of nitrogen in air. Three configurations of

129   biogas fed solid oxide fuel cell micro-combined heat and power (micro-CHP) systems are

130   studied with a particular emphasis on the application for single-family detached dwellings by

131   Farhad et al. [27]. Tjaden et al. [28] investigated a small scale biogas-SOFC plant in 2014.

132   Results show that the maximum electrical efficiency is calculated 56.55% which is 15% higher

133   than that of the combustion engines fueled by biogas. Also, the advantages and disadvantages of

134   different reforming process such as steam reforming and auto thermal reforming are reported.

135   The results revealed that the cell design voltage is higher than the cell voltage at which the

136   minimum number of cells is obtained for the SOFC stack. Also, the maximum electrical

137   efficiency of 42.7% is obtained for one of the configurations. Producing biogas from biomass

138   and then feeding either the SOFC or internal combustion engine is studied by Santarelli et al.

139   [29]. Optimization results revealed that produced electrical energy for the SOFC is higher than

140   that for the internal combustion engine where the consumed thermal energy is the same for both

141   systems. Papurello et al. [30] studied the performance of a biogas-fed SOFC power plant

142   experimentally. A 500 W_{el} SOFC stack was installed at a biomass digester pilot plant and was

143   fed with real biogas for more than 400 hours, after which a stable voltage was achieved under

144   partial oxidation reforming conditions. The fuel utilization was approximately 55% and the

145   electrical efficiency was close to 34%. The biogas which is obtained from organic waste

146   collection from local municipal areas via digester consists of methane and carbon dioxide

147   concentrations ranging from 60-70% and 30-40% vol., respectively. Trendewicz and Braun [31]

148   analyzed a biogas-fueled solid oxide fuel cell (SOFC) system for producing heat and power from

149   the view point of techno-economic. They estimated that the baseline cost of electricity for the

150   small, the medium, and the large plants is 0.079 $/kWh, 0.058 $/kWh and 0.05 $/kWh,

151   respectively. Gandiglio et al. [32] proposed a model to analyze the integration of waste water

152   treatment (WWT) biogas and solid oxide fuel cell considering both the internal and external

153   reforming. The influence of fuel utilization, internal reforming, biogas composition and steam-

154   to-carbon ratio on both the SOFC and overall plant performance is investigated. It is observed

155   that an increase in the methane concentration of biogas would increase the electrical efficiency of

156   the plant slightly. Siefert and Litster [33] investigated the performance of a biogas-fed SOFC

157   from the viewpoint of economics. Their interesting result may be the one revealing that the

158   anaerobic digestion-SOFC system is significantly more economic than the systems in which the

159   biogas is sent to internal combustion engines or micro gas turbines. An exergoeconomic analysis

160   of biogas-fed SOFC power systems focusing on the (anode/cathode) gas recycling investigated

161   by Mehr et al. [34]. It is reported that, the solid oxide fuel cell system with anode and cathode

162   recycling is superior to the other configurations and its efficiency is calculated as 46.09% being

163   6.81% higher than that of the simple solid oxide fuel cell fed by natural gas. The unit product

164   cost of the solid oxide fuel cell system with anode and cathode gas recycling is calculated as

165   19.07$/GJ which is about 35% lower than the corresponding value for the simple natural gas fed

166   solid oxide fuel cell system.

167   As discussed above, there are two common ways to produce gas from the biomass, using

168   gasifier or digester. In the present work, a downdraft gasifier and a thermophilic digester are

169   used to produce syngas and biogas from the municipal solid waste, respectively. The produced

170   gases are supposed to drive the SOFC system to produce power. As the compositions of biogas

171   and syngas are quite different, and also the exhaust of SOFC is hot enough, the CHP system

172   would be an interesting choice to utilize the hot exhaust of SOFC stack to produce heating. Also,

173   it would be interesting to reveal which system is more efficient and more economical with the

174   almost same working conditions. Modeling of the systems is performed in EES software and the

175   performance of systems is compared with each other from the thermodynamics and thermo-

176   economics viewpoints.

177   2. System description and assumptions

178   2.1 Systems configuration

179   Schematic diagram of the proposed cogeneration system based on the digester unit system is

180   illustrated in Fig.1a. The system consists of a biogas production unit, a SOFC with anode

181   recycling and heat recovery steam generator (HRSG). Biomass is sent to the digester at

182   environmental conditions and as the digester is considered thermophilic one the temperature of

183   biogas exiting the digester will be higher than environment temperature. Then the biogas is sent

184   to the cleanup unit, in which H_2S is coldly removed and then the clean biogas is sent to the

185   blower. The biogas and air are preheated through the fuel heat exchanger and air heat exchanger,

186   respectively, after being pressurized with the help of fuel and air blowers (the pressure is just to

187   make a flow of fuel and air and compensate the pressure drops within the system). The heated air

188   is sent to the cathode of the stack. On the other hand, the biogas is sent to the anode after mixing

9

189   with the recycling of anode stream (state15). The mixed stream experiences the internal

190   reforming process which brings hydrogen-rich products participating in the electrochemical

191   reaction inside the fuel cell stack. An inverter is used to convert the DC power generated by the

192   stack into grid quality electricity. The electrochemical reaction generates thermal energy a part of

193   which is used to deliver the required heat of the internal reforming reaction, another part is

194   employed to heat up the cell products and residual reactants, and the remaining small amount is

195   transferred to the environment as a heat loss (in the present modeling heat loss is neglected).

196   After the finishing of electrochemical reaction in the SOFC stack, the excess air out of the

197   cathode and the unreacted fuel out of the anode combust completely in an after-burner to

198   generate the combustion gas under high temperature. The exhaust gas from the afterburner is

199   sequentially used to preheat the fuel and air, respectively. The exhaust (state 15) is still hot

200   enough to be utilized to produce hot steam. Therefore, a HRSG unit is considered to be coupled

201   with SOFC system. For the maintenance of the digester temperature in the thermophiles

202   condition, the produce hot water can be used to compensate the heat demand of digester. Fig. 1b

203   depicts the use of syngas produced in the gasification process to produce power and heating by

204   means of SOFC power plant and HRSG unit. The description of the process for the system is

205   almost the same as described for the Fig. 1a. The air from environment is brought to the gasifier

206   along with the biomass in the atmospheric pressure. The equilibrium model is presumed in

207   modeling the gasifier. The equilibrium modeling assumes that all the reactions are in

208   thermodynamic equilibrium and that the pyrolysis product (gas) which is product of interest

209   burns and achieves equilibrium in the reduction zone before leaving the downdraft gasifier.

210   Meanwhile, the high temperature syngas produced in gasifier first used to preheat the air before

211   sending it to the mixer to be mixed with anode gas recycle.

212   2.2 Assumptions

213   Some meaningful assumptions are considered for the systems modeling as listed below

214   [35,36];

215   • The atmospheric air is composed of 79% N_2 and 21% O_2, on a volume basis.

216   • Gasification temperature is assumed to be 1073 K and the syngas is in thermodynamic

217   equilibrium

218   • A thermophilic digester is used in the modeling

219   • Fan work in the digester is negligible

220   • All gases are treated as ideal gases and gas leakage from the components and the connecting

221   pipes is negligible.

222   • The analysis is carried out under thermodynamic equilibrium and steady state conditions.

223   • Changes in kinetic and potential energies are neglected.

224   • Temperatures at channel inlets are the same and, similarly, temperatures at the channel exits

225   are the same.

226   • The fuel cell is insulated perfectly so that there is no heat interaction with the environment

227   • Contact resistances are negligible.

228   • Unreacted gases are assumed to be fully oxidized in the afterburner. [37]

229   The input data for systems' simulation are listed in Table 1.

230   # 3. Energy analysis

231   ## 3.1 Gasifier modeling

232   The equilibrium model presumed in gasifier modeling assumes that all the reactions are in

233   thermodynamic equilibrium and that the pyrolysis product burns and achieves equilibrium in the

234   reduction zone before leaving the downdraft gasifier [36]. The reactions in the reduction zone

235   are as stated in the literature [36,38,39].

$$CH_aO_bN_c + wH_2O + m(O_2 + 3.76N_2) \\ \rightarrow n_1H_2 + n_2CO + n_3CO_2 + n_4H_2O + n_5CH_4 + n_6N_2 \tag{1}$$
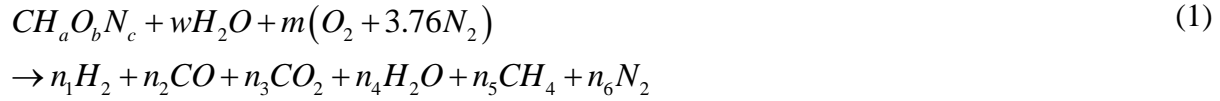
236   For a biomass, the global gasification reaction is as follows [40]:

237   The equilibrium constants for methane formation reaction and for the water-gas reaction (shift

$$K_1 = \frac{n_5}{n_1^2}\left(\frac{P/P_{ref}}{n_{tot}}\right)^{-1} \tag{2}$$

$$K_2 = \frac{n_1 n_3}{n_2 n_4}\left(\frac{P/P_{ref}}{n_{tot}}\right)^{0} \tag{3}$$

238   reaction) are given by Eqs. 2 and 3, respectively [38]:

239   where n_1 to n_5 are the number of moles in the gasification products in eq. 1. and K_1 and K_2 are

240   the equilibrium constants which can be related to the change in the Gibbs function as follows

241   [38]:

$$\frac{-\Delta G_1^0}{\overline{R}T_g} = ln\,K_1 \tag{4}$$

242

$$\frac{-\Delta G_2^0}{\bar{R}T_g} = \ln K_2 \qquad (5)$$

243   Where $-\Delta G_1^0$ and $-\Delta G_2^0$ are the change in the Gibbs free function of methane formation equation

244   and shift reaction respectively[36].

245   In Eq. 1, $CH_aO_bN_c$ denotes the biomass, w is the biomass moisture content and m is the kmol of

246   oxygen per kmol of biomass. The parameter m is actually the air fuel ratio and can be determined

247   if the gasification temperature is known (or vice versa). The coefficients n_1 to n_6 are determined

248   through applying the mass balance for H, C, O and N. Based on the ultimate analysis of the

249   MSW as given in Table 2.

250   The moisture content per mole of biomass can be expressed in terms of mass based moisture

251   content (MC) as follows [36]:

$$w = \frac{M_{biomass}\,MC}{18\,(1-MC)} \qquad (6)$$

252   where,

253   MC = (mass of water/mass of wet biomass)$\times$ 100

254   Assuming an adiabatic gasification at a temperature of 1073 K, the energy balance equation, as

$$\begin{aligned}
\bar{h}_{f-MSW}^0 + w\,(\bar{h}_{f-H_2O}^0) &= n_1\left(\bar{h}_{f-H2}^0 + \Delta\bar{h}_{H_2}\right) + n_2\left(\bar{h}_{f-CO}^0 + \Delta\bar{h}_{CO}\right) \\
&+ n_3\left(\bar{h}_{f-CO2}^0 + \Delta\bar{h}_{CO2}\right) + n_4\left(\bar{h}_{f-H2O}^0 + \Delta\bar{h}_{H2O}\right) + n_5\left(\bar{h}_{f-Ch4}^0 + \Delta\bar{h}_{Ch4}\right) + n_6\left(\bar{h}_{f-N2}^0 + \Delta\bar{h}_{N2}\right)
\end{aligned} \qquad (7)$$

255   indicated below, is solved to find the air fuel ratio.

256   In order to validate the gasification model, the experimental and theoretical data reported in

257 the literature are used for gasification temperature of 1100K and moisture content of 16%. The

258 comparison is shown in Table 3. Referring to Table 3, the sum of hydrogen and carbon

259 monoxide content percentages predicted by the present model is 36.43%, which agrees with the

260 experimental data (35.4%) reported by Jayeh [41]. It is found that the obtained results for the

261 present model agree well with those reported by Jarungthammachote [42] as well.

262 In order to validate the simulation results of SOFC, the available experimental data reported

263 by Tao et al. [43] is used. Table 4 compares the cell voltage and power density obtained in the

264 present model developed by the authors and those reported by Tao et al. [43]. The comparison

265 shows a good agreement between them.

266 3.2 Digester modeling

267 In modeling of digester, a thermophilic anaerobic digester with a temperature of 55°C is used.

268 Note that, it is necessary that temperature fluctuations do not occur in the digester to maintain the

269 microbial activity.

270 With knowledge of chemical composition of MSW outlined as ultimate analysis in Table 2

271 the biogas composition can be predicted following the method proposed by Baswell and Hatfield

272 [44]. The global reaction occurring in the digester to produce biogas is:

$$C_nH_aO_b + wH_2O \rightarrow n_1CO_2 + n_2CH_4 \tag{8}$$

273 In the present work, it is assumed that 0.95 of the OFMSW is volatile. A well designed

274 digester aims to destruct at minimum 0.7 of the volatile solid. Following the procedure presented

275 by Murphy[45] the methane and carbon dioxide mass is found. Knowing that the number of

276 molecules in a unit volume under standard conditions is the same for all gases (This volume is

277 22.412m^3/kg) one may find that the 58% of the biogas is methane and 42% of biogas is carbon

14

278   dioxide in volume.

3.3 SOFC with anode recycle model

280   Energy analysis and molar balance for the SOFC with anode and cathode recycle is used in

281   the present work. [46][46]The biogas is converted into a hydrogen-rich synthesis gas inside the

282   fuel cell by making use of internal reforming and shifting reactions [35]. Also syngas (with

283   hydrogen gas) which does not need any reforming and less methane and carbon monoxide gas is

284   reformed inside the SOFC with the same processes as for biogas. The use of an internal reformer

285   also reduces the dependence of the fuel cell on a cooling system. The chemical reactions in the

286   cells are as follows; [47]

$$CH_4 + H_2O \rightarrow CO + 3H_2 \quad \text{(Reforming)} \tag{9}$$

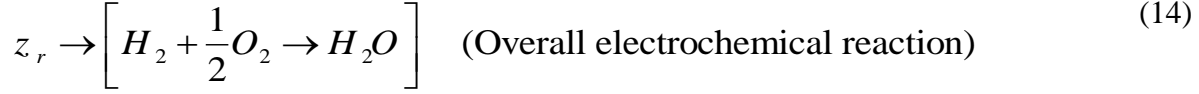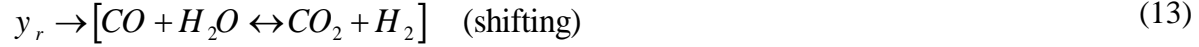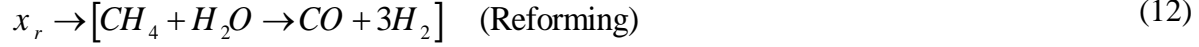$$CO + H_2O \rightarrow CO_2 + H_2 \quad \text{(Shifting)} \tag{10}$$

287   Equation 9 is reforming reaction and equation 10 is shifting reaction, carbon monoxide in the

288   reforming reaction, reacts with the water which is brought to the SOFC by means of either

289   recycling or externals means such as pump, to produce hydrogen. Hydrogen from shifting

$$H_2 + \frac{1}{2}O_2 \rightarrow H_2O \quad \text{(overall electrochemical reaction)} \tag{11}$$
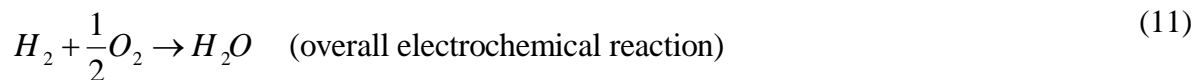
290   reaction is used in the electrochemical reaction as below:

291   The molar conversion rates for reforming, shifting and electrochemical reactions are

292   considered to be x_r, y_r, and z_r, respectively. Therefore, rates of consumption and production of

293   the components can be achieved by the following model:

15

$$x_r \rightarrow \left[CH_4 + H_2O \rightarrow CO + 3H_2 \right] \quad \text{(Reforming)} \tag{12}$$

$$y_r \rightarrow \left[CO + H_2O \leftrightarrow CO_2 + H_2 \right] \quad \text{(shifting)} \tag{13}$$

$$z_r \rightarrow \left[H_2 + \frac{1}{2}O_2 \rightarrow H_2O \right] \quad \text{(Overall electrochemical reaction)} \tag{14}$$

294   z_r, could be found with the help of current density, Faraday constant, cell number, and active

$$z_r = \frac{j \, N_{FC} \, A_a}{2F} \tag{15}$$

295   surface area, as followed by equation (16)

296   Applying mass balance equations along with considering equations 13-16 for the mixing units

297   and the whole SOFC model the flowing gas compositions may be achieved. In order to solve the

298   system of equations, 3 more equations are needed to complete the system of the equations.

299   Looking again in the equilibrium reactions of shifting and reforming, the equilibrium constants

$$\ln K_s = -\frac{\Delta \bar{g}_s^o}{\bar{R} T_{FC,e}} = \ln \left[\frac{(\dot{n}_{CO_2,11} + y_r)(\dot{n}_{H_2,11} + 3x_r + y_r - z_r)}{(\dot{n}_{CO,11} + x_r - y_r)(\dot{n}_{H_2O,11} - x_r - y_r + z_r)} \right] \tag{16}$$

$$\ln K_R = -\frac{\Delta \bar{g}_R^o}{\bar{R} T_{FC,e}} = \ln \left[\frac{(\dot{n}_{CO,11} + x_r - y_r)(\dot{n}_{H_2,11} + 3x_r + y_r - z_r)^3}{(\dot{n}_{CH_4,11} + x_r)(\dot{n}_{H_2O,11} - x_r - y_r + z_r) \times \dot{n}_{12}^2} \left(\frac{P_{12}}{P_{ref}} \right)^2 \right] \tag{17}$$

300   can be written as follows respectively:

301   Where, $\bar{R}$ and $T_{FC,e}$ are the universal gas constant and the temperature at the exit of the

302   SOFC, respectively. Also, $\Delta \bar{g}^o$ is the change in the Gibbs free function of shifting and reforming

16

303 reactions[35].

304 The last equation needed for solving the system equations is obtained using the energy

305 balance for the whole stack. Neglecting the heat loss from the stack, the energy balance can be

$$\dot{W}_{FC,stack} = \sum_{k} \dot{n}_{k,12}\bar{h}_{k,12} + \sum_{L} \dot{n}_{L,4}\bar{h}_{L,4} - \sum_{m} \dot{n}_{m,11}\bar{h}_{m,11} - \sum_{n} \dot{n}_{n,3}\bar{h}_{n,3} \qquad (18)$$

306 written as follows;

307 Where, k, L, m and n are the corresponding gas compositions in each states (e.g. gas

308 composition at state 12 (L) is CO_2, CO, H_2O, CH_4, N_2 and H_2)). On the other hand, the work rate

$$\dot{W}_{FC,stack} = N_{FC}\ j\ A_a V_c \qquad (19)$$

309 produced by the SOFC stack $\dot{W}_{FC,stack}$ can be expressed as:

$$V_c = V_N - V_{loss} \qquad (20)$$

310 Where cell voltage is defined as:

311 Here, V_N is the Nernst voltage and V_{loss} the voltage loss, which is the sum of three separate

312 voltage losses; Ohmic, Activation and Concentration losses:

$$V_{loss} = V_{ohm} + V_{act} + V_{conc} \qquad (21)$$

313 Looking again in the comprehensive analysis of the cell voltage and voltage losses it is found

314 that voltages strongly depend on molar fractions, pressures, electrolyte types and cell operating

315   temperature that need to be verified very precisely. For the sake of brevity detailed voltage

316   modeling used in the present work has been presented in Appendix A.

317   3.4 Heat recovery steam generator analysis

318   One of the determinant parts of the proposed systems is HRSG, which affects the final system

319   specifications and has crucial effect on determining whether to choose gasifier or digester. Gas

320   flow from the AHX is hot enough that can be utilized to generate saturated steam in HRSG. As

321   shown in Fig. 1a and Fig. 1b the HRSG involves economizer (Eco) and evaporator (Eva) parts.

322   Water is pressurized by a pump (P) to meet the required steam pressure for the HRSG.

323   Applying the energy balance as well as the pinch point temperature difference for the whole

324   HRSG system the mass flow rate of steam and temperature of exhaust can be determined. Energy

325   balance for the economizer and the evaporator parts are as follows:

$$\sum_{j} n_j \left(\bar{h}_{f_j}^0 + \Delta\bar{h} \right)_{exhaust\ gas\ ,in} + n_{water,in}\ \bar{h}_{water,in} = \sum_{j} n_j \left(\bar{h}_{f_j}^0 + \Delta\bar{h} \right)_{exhaust\ gas\ ,out} + n_{water,out}\ \bar{h}_{water,out} \tag{22}$$

326   Where the amount of heat used for generating hot steam is defined as;

$$\dot{Q}_{Heating} = \dot{m}_{product\ gas}(h_{15} - h_{17}) \tag{23}$$

327   3.5. First law efficiency for proposed system

328   Finally with regarding the above mentioned analysis, the first law efficiency for the power

329   generation (electrical efficiency) mode and CHP mode could be defined as follows respectively:

$$\eta_{I,P} = \frac{\dot{W}_{FC,stack,ac} - \dot{W}_{FC} - \dot{W}_{AC} - \dot{W}_{pump}}{\dot{m}_{biomass}\ LHV_{biomass}} \tag{24}$$

$$\eta_{\text{I,CHP}} = \frac{\dot{W}_{FC,stack,ac} - \dot{W}_{FC} - \dot{W}_{AC} - \dot{W}_{pump} + \dot{Q}_{Heating}}{\dot{m}_{biomass} LHV_{biomass}} \tag{25}$$

330 Where $\dot{W}_{FC}, \dot{W}_{AC} \text{ and } \dot{W}_{p}$ is the amount of fuel compressor power and air compressor power

331 required to blow the fuel and air to the SOFC and pump required power respectively.

4. Exergy analysis

333 An effective use of energy can be assessed by means of exergy analysis for energy converting

334 systems. Exergy can be divided into four parts: physical, chemical, kinetic and potential

335 exergies. For the processes involved in this paper, the latter two are neglected since the changes

336 in elevation and velocity are negligible [48,49]. Thus, the specific exergy of any stream is

337 expressed as

$$e = e_{ph} + e_{ch} \tag{26}$$

338 where the physical exergy is defined as [48] :

$$e_{ph,i} = h_i - h_0 - T_0 \left(s_i - s_0 \right) \tag{27}$$

339 The specific chemical exergy of a solid biomass fuel can be expressed as follows [36]:

$$e_{biomass}^{ch} = \beta LHV_{biomass} \tag{28}$$

340 where the factor β in Eq. 28 denotes the ratio of the chemical exergy to the lower heating value

341 (LHV) for the organic fraction of the biomass. A statistical correlation for the β is provided by

342 Szargut and Styrylska [36]:

19

$$\beta = \frac{1.044 + 0.16\frac{z_H}{z_c} - 0.34493\frac{z_o}{z_c}\left(1 + 0.0531\frac{z_H}{z_c}\right)}{1 - 0.4142\frac{z_o}{z_c}} \tag{29}$$

343 where z_H, z_c, z_o are the weight fractions of the hydrogen, carbon and oxygen in the biomass,

344 respectively. The chemical exergy of an ideal gas mixture can be expressed as [48]:

$$e_i^{ch} = \sum_i x_i e_{0,i}^{ch} + \bar{R}T_0 \sum_i x_i lnx_i \tag{30}$$

345 where x_i is the mole fraction of i_{th} component and $e_{0,i}^{ch}$ is the standard chemical exergy of that

346 component [38]. The exergy balance for a system component is expressed as:

$$\sum \dot{E}_{In} = \sum \dot{E}_{out} + \dot{E}_D \tag{31}$$

347 With the aid of eq. 31 one may find the exergy destruction in system components in order to

348 define the most probable candidate of optimizing for higher efficiency.

349 Finally, exergy analysis can be completed by defining the efficiency of second law for the power

350 generation (electrical efficiency) mode and CHP mode as follows:

$$\eta_{II,P} = \frac{\dot{W}_{FC,stack,ac} - \dot{W}_{FC} - \dot{W}_{AC} - \dot{W}_{pump}}{\dot{E}_{in}} \tag{32}$$

$$\eta_{II,CHP} = \frac{\dot{W}_{FC,stack,ac} - \dot{W}_{FC} - \dot{W}_{AC} - \dot{W}_{pump} + (\dot{E}_{22} - \dot{E}_{20})}{\dot{E}_{in}} \tag{33}$$

351 where $\dot{E}_{in}$ is the rate of input exergy and can be defined as below for gasifier coupled SOFC

352 and digester coupled SOFC respectively:

$$\dot{E}_{in} = e_{biomass}^{ch} + w\, e_{water}^{ch} + 4.76m\, e_{air}^{ch} + \dot{E}_6 + \dot{E}_{19} \tag{34}$$

20

$$\dot{E}_{in} = e_{biomass}^{ch} + w\ e_{water}^{ch} + \dot{E}_{19} \qquad (35)$$

5. Economic analysis

5.1. Methodology

It seems that investigating the performance of a system without looking at its product cost will not be accomplished. Integration of economic point of view with thermodynamic seems to be appealing. Exergoeconomic method firstly introduced by Tsatsaronis et al. [50] gets the interest of researchers who use the method to analyze the thermodynamic systems from the viewpoint of economic. The purpose of exergoeconomic analysis for a system is to disclose the cost formation processes and calculate the cost per unit exergy of product streams. To calculate the cost of each unit exergy stream, the cost balance equation along with the required auxiliary equations are applied to each component of the systems. For a system component receiving thermal energy and generating power, the cost balance is written as:

$$\sum \dot{C}_{out,k} + \dot{C}_{w,k} = \sum \dot{C}_{in,k} + \dot{C}_{q,k} + \dot{Z}_{k,PY} \qquad (36)$$

$$\dot{C} = c\ \dot{Ex} \qquad (37)$$

Where, c is the cost per exergy unit and $\dot{Ex}$ is the total exergy rate.

In equation (36), $\dot{Z}_{k,PY}$ is the appropriate charge due to capital investment and operating and maintenance expenses for each component in a reference year. Note that, the cost of the system components which are available in an original year is converted from that original time to a same reference year (year 2013 for present work) with the help of Chemical Engineering Plant Cost Index (CEPEI).

$$\dot{Z}^o_k = \dot{Z}^{o,CI}_k + \dot{Z}^{o,OM}_k \tag{38}$$

370   Cost at reference year=Original cost $\times \dfrac{\text{Cost index for the reference year}}{\text{Cost index for the original year}}$

371   Or

$$\dot{Z}_{k,PY} = \dot{Z}^o_k \frac{CI_{k,PY}}{CI^o} \tag{39}$$

372

373   The term $\dot{Z}^o_k \dot{Z}_k$ in Eq. (38) can be calculated as [48]:

$$\dot{Z}^o_k = \frac{Z_k\,CRF\,\varphi}{N} \tag{40}$$

374   Where φ is the maintenance factor, N is the number of system operating hours in a year and

375   CRF is the Capital Recovery Factor, which can be expressed as [51]:

$$CRF = \frac{i_r\left(1+i_r\right)^n}{\left(1+i_r\right)^n - 1} \tag{41}$$

376   Here, i_r is the interest rate and n is the system life. The input data used in economic

377   evaluations along with the cost and auxiliary equations for each component of the systems is

378   gathered in Table 5.

379   5.2 Cost evaluation

380   To obtain the cost of all unit exergy streams, the linear system of equations is solved

381   assuming that the cost of unit exergies associated with the input fuel is an input.

382   The exergoeconomic evaluation of the systems is carried out using the thermoeconomic

383   variables, namely, the unit cost of the fuel ($c_{F,k}$), the unit cost of the product ($c_{P,k}$), the cost rate of

384   exergy destruction ($\dot{C}_{D,k}$), the cost rate of exergy loss ($\dot{C}_{L,k}$) and the thermoeconomic factor (f_k).

385   These parameters are calculated using the following relations [48]:

6. Results and discussions

386

387   The effect of decision parameters such as the current density, the temperature difference of

388   SOFC stack on efficiencies of power generating system and CHP system along with net power

389   output, heating capacity and unit product cost of the systems is investigated. Nominal values of

390   current density, where maximum power is achieved, are found to be 0.6 mA/cm^2 and 0.2

391   mA/cm^2 for the D-SOFC and G-SOFC systems respectively.

392   Fig. 2 shows the effect of current density on the first and second law efficiencies of the power

393   generating system. Referring to Fig. 2, the current density range is lower for G-SOFC system

394   because of N$_2$ presence in the gasifier exit, which causes partial pressure of components in stack

395   exit to become less than the D-SOFC system and it affects the cell voltage due to decrease in J$_{0a}$.

396   Looking again in Fig 2, for constant value of fuel utilization factor both first and second law

397   efficiencies tend to decrease with increasing current density. With increasing 0.6 A/cm^2 in

398   current density for the D-SOFC system, first and second law efficiencies tend to decrease by an

399   almost 40%. While the reduction is about 30% for the G-SOFC system (with a possible increase

400   of 0.2 A/cm^2).

401   Fig. 3a shows the effect of current density on the first and second law efficiencies of the CHP

402   system. The results show that the first law efficiency for the G-SOFC system is in the range of

403   50%- 74% while the efficiency for the D-SOFC system is obtained in the range of 35%-84%.

404   The great difference between the first and second law efficiency values for G-SOFC system is

405   due to the exergy rate within the HRSG system (exergy related to heating).

406   Fig. 3b shows the effect of current density on both the net power output and heating capacity.

407   First important point is that, the net power output is maximized for specific values of current

408   density for both the D-SOFC and G-SOFC systems. The optimum current density value for G-

409   SOFC system is found to be 0.199 A/cm^2 and the corresponding net power output is calculated

410   46.98 kW. For the D-SOFC system the optimum current density and net power values are 0.64

411   A/cm^2 and 159.7 kW, respectively. In addition, it is observed that an increase in the current

412   density increases the heating capacity with an almost same trend of power. At the optimum

413   working points (where the net power output is maximized) the heating capacity values are

414   88.3kW and 43.31kW for the G-SOFC and D-SOFC systems, respectively. Another important

415   aspect of Fig 3b is that although the net power output is higher for the digester based system, the

416   heating capacity is higher for the gasifier system which could be interfered from contemplating

417   in Figs 3a and 3b. Also by an increase in current density, the value of heating capacity increases

418   by up to 83% and 45% for the G-SOFC system and D-SOFC system respectively.

419   Fig. 4 shows the effect of current density on the unit exergy cost of power output (c_w) and hot

420   steam (c_h) for both the D-SOFC and G-SOFC systems. It is revealed that besides the efficiency

421   of D-SOFC is higher it has come at the price of lower unit product cost. Also it is unfolded that

422   for both cases the unit product cost is minimized at some specific point. For the G-SOFC system,

423   the minimum value of unit exergy cost of heating (24.67$/GJ) occurs at current density of 0.203

424   A/cm^2 while for the case of D-SOFC system the values are 14.17 $/GJ and 0.602 A/cm^2,

425   respectively. It can be seen that even in the minimum values, the D-SOFC system is cost-

426   efficient by 41.6% and 70.2% for heating unit exergy cost and power unit exergy cost,

427   respectively.

24

428   Another key parameter having effect on the system performance is the stack temperature

429   difference. Fig. 5 shows the effect of stack temperature difference on second law efficiency of

430   CHP and power generation systems for both the D-SOFC and G-SOFC systems. Second law

431   efficiency for the D-SOFC system is always higher than that for the G-SOFC system but

432   important aspect of this figure is that variation of second law efficiency for power generation

433   mode and CHP mode of G-SOFC tends to decrease after a specific value of temperature. This is

434   actually due to the different composition of inlet gas sent to the anode and consequently different

435   partial pressure of H_2 and H_2O at the anode exit. As the stack temperature difference increases

436   110 ^{o}C, exergetic efficiency for D-SOFC system (in the CHP mode) rises by 52.9% while with

437   an increase of 90°C the efficiency of the G-SOFC system increases by 75.3%. In addition, as the

438   temperature difference increases by 80 ^{o}C the second law efficiency of power generation system

439   for the G-SOFC system rises by 25%, the change is an almost the same for the case of D-SOFC

440   with a value of 25.4%.

441   Fig. 6a shows the effect of stack temperature difference on the net power output and heating

442   capacity for the D-SOFC and G-SOFC systems. Comparing the G-SOFC and D-SOFC systems,

443   net power output of G-SOFC system increases by 27.60% with an increase in stack temperature

444   difference and for the D-SOFC system the increase is 25.5%. The trend of heat duty is different

445   as with an increase in temperature of stack results in an increase of exhaust potential of SOFC

446   system which would be utilized in HRSG system. Although the trend seems to be similar for two

447   cases, for the D-SOFC system the percentage of increase is much higher compared to the G-

448   SOFC system.

449   Fig. 6b shows the effect of stack temperature difference on unit exergy costs of heating

450   capacity and power output for both the D-SOFC and G-SOFC systems. It is revealed that for the

25

451 D-SOFC system unit heating product cost is minimized at stack temperature difference of 183 K

452 which corresponds to unit cost of 9.18 $/GJ while the stack temperature difference and unit cost

453 values are 135.6 K and 16.1 $/GJ for the G-SOFC system. Also, at the minimum point the D-

454 SOFC system has 75.3% less unit product cost in heating and 91.31% in power unit product cost

455 compared to the G-SOFC system.

456 Finally to give an insight of overall product cost variation with terminal temperature

457 differences of SOFC stack Fig. 6c is presented. It shows that the with a change of about $100\,^{\circ}C$ in

458 stack temperature difference, the minimum unit product cost of G-SOFC system is more than the

459 maximum unit product cost of D-SOFC system.

460 Fig. 7a and Fig. 7b illustrate the G-SOFC and D-SOFC systems' calculated parameters at

461 nominal operating condition and stack temperature difference equal to $100\,^{\circ}C$. According to Fig.

462 7a the second law efficiency for the D-SOFC system is higher with a value of 97.8% in power

463 generation system and 57.7% in CHP system. The difference becomes less in CHP system due to

464 higher heating capacity in G-SOFC system, moreover considering the results illustrated in Fig.

465 7b it is found that the unit product cost for G-SOFC system for power generation system and

466 CHP system is 42.6% and 24.5% more than those for the D-SOFC system respectively. Fig. 7b

467 shows the value of net output power and heating capacity as well as the unit product cost for

468 power and heating for the two proposed systems at the same working conditions. Fig.7b shows

469 that the G-SOFC system has 111 kW less power output and 45.9kW more heating load than the

470 D-SOFC system.

471 One method to illustrate exergy accounting graphically is the Grassman diagram [48]. The

472 width of the arrows entering or leaving the control volume is a quantitative measure of

473 designated parameter. Also for the sake of brevity, values of exergy destruction along with

26

474 entering and leaving exergy to the whole system are presented in Table 6. According to the Figs.

475 8a and 8b and Table 6, one may conclude that the air heat exchanger and the gasifier are the

476 main sources of irreversibility due to the existence of three sources of irreversibility (temperature

477 difference, chemical reaction along with system friction) within these components in the D-

478 SOFC and G-SOFC systems respectively.

479 Table 7 and Table 8 show the exergoeconomic analysis results for the G-SOFC and D-SOFC

480 systems. Last column of these tables is exergoeconomic factor which a low value of this factor

481 calculated for a major component suggests that cost saving in the entire system *might* be

482 achieved by improving the component efficiency (reducing exergy destruction) even if the

483 capital investment for the component will increase. However, the exergoeconomic factor is not

484 sufficient to explain if a component has to be modified or not. As an example: even if a

485 component has a too low value of exergoeconomic factor (suggesting therefore its substitution

486 with a component of higher performance and higher cost) if the same component elaborates a

487 quantity of fuel which is negligible (and so it has a low value of the so called exergetic factor) it

488 is not worth at all to substitute this component with a better one, as its "exergy role" on the

489 system is simply negligible. The most important components to discuss are the components

490 elaborating a large amount of inlet fuel (so, which have a high value of exergetic factor): only in

491 their case it is interesting to analyze the values of their exergoeconomic factor. Referring to first

492 column of Tables 7 and 8, it can be noted that for the gasifier based system, among the

493 components having higher inlet exergy (SOFC stack, gasfier, after burner and AHX respectively)

494 the SOFC stack and AHX have the highest (88.75%) and lowest (16.02%) exergoeconomic

495 factors, respectively. Therefore, for the case of G-SOFC system, on the one hand, engineers

496 should focus on reducing the investment and operation costs of SOFC stack and on the other

497 hand, they are to reduce the costs associated with exergy destruction for the AHX. The same

498 point can be stated for the case of D-SOFC. Therefore, for the D-SOFC and G-SOFC systems,

499 not only designers should emphasize on decreasing the investment cost of SOFC stack but also

500 reducing the cost associated with exergy destruction within the air heat exchangers should be in

501 priority.

502 Finally at the end, a summary of plant type, fuel type and technology of using biomass to

503 produce gas to feed SOFC power plant in some published works as well as those proposed and

504 obtained in the present work are listed in Table 9. Comparison shows that most of the published

505 works focused on just one technology (gasification to produce syngas or digestion to produce

506 biogas) to utilize the biomass. Also there are few works that comprehensively analyzed the

507 system from the both of thermodynamic and techno economic point of view. However, in the

508 present work, the investigation has been made to fulfill this gap and the thermodynamic and

509 economic analyses are performed to compare two well-known technologies of using biomass in

510 the SOFC system.

7. Conclusion

511

512 A comprehensive thermodynamic and thermoeconomic modeling are performed for two

513 proposed cogeneration systems based on SOFC system fed by municipal solid waste. The inlet

514 fuel for the SOFC is a type of syngas produced by gasification process of municipal solid waste

515 or a biogas produced by digestion process. For the comparison purposes, the systems analyzed in

516 two modes; one-generation system (produce power) and a CHP mode (producing power and

517 heating simultaneously). Parametric studies revealed that stack temperature difference along with

518 current density has crucial effect on systems' performance. Additional conclusions are as

519   follows:

520   • D-SOFC system has higher efficiency from the viewpoints of energy and exergy when

521   the systems run to produce power.

522   • D-SOFC system has higher second law efficiency in CHP mode; however the first law

523   efficiency for the G-SOFC is higher in this mode.

524   • D-SOFC system has more power output but less heating capacity compared to those of

525   the G-SOFC system.

526   • For the case of G-SOFC system the gasifier is the main source of irreversibility due to

527   temperature difference and chemical reaction. Meanwhile, air heat exchanger is the

528   second source of irreversibility because of large temperature difference on the both sides

529   of heat exchanger. For the D-SOFC system, air heat exchanger has the most distribution

530   in exergy destruction within the system, the stack and digester are the second and third

531   respectively.

532

533

534

535   **Appendix A**

536   Here, the electrochemical model (for calculating the cell voltage) programing in EES is given

537   in details. The cell voltage can be defined as;

$$V_c = V_N - V_{loss}$$

<div align="right">A1</div>

where, V_N is the Nernst voltage and V_{loss} is the voltage loss which is the sum of three

$$V_{loss} = V_{ohm} + V_{act} + V_{conc}$$

<div align="right">A2</div>

539   separate voltage losses (ohmic, activation, and concentration losses):

$$V_N = -\frac{\Delta \bar{g}^o}{2F} + \frac{\bar{R}T_{FC,e}}{2F} \ln\left(\frac{a_{H_2}^{Anode,exit} \sqrt{a_{O_2}^{Cathode,exit}}}{a_{H_2O}^{Anode,exit}} \right)$$

<div align="right">A3</div>

540   The Nernst voltage which is accounted as the ideal voltage can be expressed as;

541   In equation (A3), the Gibbs energy difference is related to the overall electrochemical

542   reaction. To determine the actual cell voltage, the voltage losses should be calculated. To

543   calculate the Ohmic loss the following formula is used [52];

$$V_{ohm} = (R_{Int} + \rho_{an}L_{an} + \rho_{cat}L_{cat} + \rho_{ely}L_{ely})j$$

<div align="right">A4</div>

544   where, ρ, L and R_{Int} denote electrical resistivity of a cell component, thickness of a cell

545   component and interconnection resistivity, respectively (See Table A.1).

546   The activation polarization is the sum of those defined for both the anode and cathode as

547   follows;

$$V_{act} = V_{act,a} + V_{act,c} \qquad\qquad\qquad\qquad\qquad\qquad\qquad\text{A5}$$

$$V_{act,c} = \frac{\bar{R}T_{FC,e}}{F}(\sinh^{-1}(\frac{j}{2j_{oa}})) \qquad\qquad\qquad\qquad\qquad\text{A6}$$

$$V_{act,c} = \frac{\bar{R}T_{FC,e}}{F}(\sinh^{-1}(\frac{j}{2j_{oc}})) \qquad\qquad\qquad\qquad\qquad\text{A7}$$

548   Where j_o is the exchange current density. Eqs. (A8) and (A9) are used to evaluate the values

549   of the exchange current density for the anode and the cathode, (see variables in Table A.2),

$$j_{0,a} = \gamma_{an}(\frac{RT}{2F})e^{\left(-\frac{E_{a,an}}{\bar{R}T}\right)} \qquad\qquad\qquad\qquad\qquad\text{A8}$$

$$j_{0,c} = \gamma_{cat}(\frac{RT}{2F})e^{\left(-\frac{E_{a,cat}}{\bar{R}T}\right)} \qquad\qquad\qquad\qquad\qquad\text{A9}$$

550   respectively [52].

551   Concentration loss is sum of the losses related to gas concentration occurring in the anode

$$V_{conc} = V_{conc,a} + V_{conc,c} \qquad\qquad\qquad\qquad\qquad\qquad\text{A10}$$

552   and cathode.

$$V_{conc,an} = \frac{RT}{2F}\ln(\frac{P_{H_2} P_{H_2O,TPB}}{P_{H_2O} P_{H_2,TPB}}) \qquad\qquad\qquad\qquad\text{A11}$$

553   Where

$$V_{conc,cat} = \frac{RT}{4F}\log(\frac{P_{O_2}}{P_{O_2,TPB}}) \qquad\qquad\qquad\qquad\qquad\text{A12}$$

554   And

555   where the subscript *TPB* denotes the three-phase boundary. To calculate the pressure at the

$$P_{H_2O,TPB} = P_{H_2O,an} + j \frac{R\,T\,L_{an}}{2\,F\,D^{eff}_{an,H_2}}$$

A13

556   reaction sites, the following equations have been used [52,53]:

$$P_{H_2,TPB} = P_{H_2,an} - j \frac{R\,T\,L_{an}}{2\,F\,D^{eff}_{an,H_2O}}$$

A14

$$P_{O_2,TPB} = P_{cat} - (P_{cat} - P_{O_2,cat}) \exp(j \frac{R\,T\,L_{cat}}{4F\,D^{eff}_{O_2}\,p_{cat}})$$

A15

557

558   where, $D^{eff}_{H_2}$, $D^{eff}_{H_2O}$ and $D^{eff}_{O_2}$ are the effective gaseous diffusivity through the anode (for H_2),

559   anode (for H_2O) and the cathode (for O_2), respectively. The effective gaseous diffusivity can be

$$\frac{1}{D^{eff}_{an,H_2}} = \frac{\varepsilon_{an}}{\tau_{an}} (\frac{1}{D_{H_2,K}} + \frac{1}{D_{H_2,H_2O}})$$

A16

$$\frac{1}{D^{eff}_{an,H_2O}} = \frac{\varepsilon_{an}}{\tau_{an}} (\frac{1}{D_{H_2O,K}} + \frac{1}{D_{H_2O,H_2}})$$

A17

$$\frac{1}{D^{eff}_{cat,O_2}} = \frac{\varepsilon_{cat}}{\tau_{cat}} (\frac{1}{D_{O_2,K}} + \frac{1}{D_{O_2,N_2}})$$

A18

560   calculated as [52,53];

561   Where the porosity (ε) and tortuosity (τ) of electrode materials are estimated to be 0.48 and

562   5.4, respectively. To calculate the effective gaseous diffusivity, combined ordinary and Knudsen

563   diffusion should be defined and calculated using the following equations as[52];

$$D_{H_2,K} = 97 r_{pore,an} \sqrt{\frac{T}{M_{H_2}}}$$ A19

$$D_{H_2O,K} = 97 r_{pore,an} \sqrt{\frac{T}{M_{H_2O}}}$$ A20

$$D_{O_2,K} = 97 r_{pore,cat} \sqrt{\frac{T}{M_{O_2}}}$$ A21

$$D_{H_2,H_2O} = \frac{1.43 \times 10^{-7} T^{1.75}}{\sqrt{M_{H_2,H_2O}} (V_{H_2}^{1/3} + V_{H_2O}^{1/3})^2 P}$$ A22

$$D_{O_2,N_2} = \frac{1.43 \times 10^{-7} T^{1.75}}{\sqrt{M_{O_2,N_2}} (V_{O_2}^{1/3} + V_{N_2}^{1/3})^2 P}$$ A

23

564

565 Where M is molecular weight of species, V represents diffusion volume of species. Meanwhile,

566 pore radius value (r_{pore}) is estimated to be 0.5 μm.

567

568

569

570

571

572

573

574

575

576 **References**

577

[1]   Basu P. Combustion and gasification in fluidized beds. Broken Sound Parkway NW, Suit
578
579   300: CRC press (Taylor and Francis); 2006.
580

[2]   Basu P. Biomass gasification, pyrolysis and torrefaction: practical design and theory. 2nd
581
582   ed. 32 Jamestown Road, London NW1 7BY, UK: Academic press (Elsevier); 2013.
583

[3]   Mckendry P. Energy production from biomass (part 3): gasification technologies.
584
585   Bioresour Technol 2002;83:55–63.
586

[4]   Mckendry P. Energy production from biomass (part 1): overview of biomass. Bioresour
587
588   Technol 2002;83:37–46.
589

[5]   Mckendry P. Energy production from biomass (part 2): conversion technologies.
590
591   Bioresour Technol 2002;83:47–54.
592

[6]   Soltani S, Yari M, Mahmoudi SMS, Morosuk T, Rosen MA. Advanced exergy analysis
593
594   applied to an externally-fired combined-cycle power plant integrated with a biomass
595   gasification unit. Energy 2013;59:775–80.
596

[7]   Saidur R, Abdelaziz EA, Demirbas A, Hossain MS, Mekhilef S. A review on biomass as a
597
598   fuel for boilers. Renew Sustain Energy Rev 2011;15:2262–89.
599

[8]   Yoshioka T, Hirata S, Matsumura Y, Sakanishi K. Woody biomass resources and
600
601   conversion in Japan: The current situation and projections to 2010 and 2050. Biomass and
602   Bioenergy 2005;29:336–46.
603

[9]   Sebastián F, Royo J, Gómez M. Cofiring versus biomass-fired power plants: GHG
604
605   (Greenhouse Gases) emissions savings comparison by means of LCA (Life Cycle
606   Assessment) methodology. Energy 2011;36:2029–37.
607

[10]   Karamarkovic R, Karamarkovic V. Energy and exergy analysis of biomass gasification at
608
609   different temperatures. Energy 2010;35:537–49.
610

[11]   Soltani S, Mahmoudi SMS, Yari M, Rosen MA. Thermodynamic analyses of a biomass
611
612   integrated fired combined cycle. Appl Therm Eng 2013;59:60–8.
613

[12]   Warnecke R. Gasification of biomass: comparison of fixed bed and fluidized bed gasifier.
614

34

615   Biomass and Bioenergy 2000;18:489–97.
616

617   [13] Knoef HAM. Inventory of biomass gasifier manufacturers and installations. Final Report
618   to European Commission. Contract DIS/1734/98-NL, Biomass Technol Gr BV, Univ
619   Twente, Enschede 2000.
620

621   [14] Omosun AO, Bauen A, Brandon NP, Adjiman CS, Hart D. Modelling system efficiencies
622   and costs of two biomass-fuelled SOFC systems. J Power Sources 2004;131:96–106.
623

624   [15] Singh D, Hernández-Pacheco E, Hutton PN, Patel N, Mann MD. Carbon deposition in an
625   SOFC fueled by tar-laden biomass gas: A thermodynamic analysis. J Power Sources
626   2005;142:194–9.
627

628   [16] Athanasiou C, Coutelieris F, Vakouftsi E, Skoulou V, Antonakou E, Marnellos G, et al.
629   From biomass to electricity through integrated gasification/SOFC system-optimization
630   and energy balance. Int J Hydrogen Energy 2007;32:337–42.
631

632   [17] Colpan CO, Dincer I, Hamdullahpur F. Thermodynamic modeling of direct internal
633   reforming solid oxide fuel cells operating with syngas. Int J Hydrogen Energy
634   2007;32:787–95.
635

636   [18] Jang H, Ocon JD, Lee S, Lee JK, Lee J. Direct power generation from waste coffee
637   grounds in a biomass fuel cell. J Power Sources 2015;296:433–9.
638

639   [19] Pieratti E, Baratieri M, Ceschini S, Tognana L, Baggio P. Syngas suitability for solid
640   oxide fuel cells applications produced via biomass steam gasification process:
641   Experimental and modeling analysis. J Power Sources 2011;196:10038–49.
642

643   [20] Di Carlo A, Bocci E, Naso V. Process simulation of a SOFC and double bubbling
644   fluidized bed gasifier power plant. Int J Hydrogen Energy 2013;38:532–42.
645

646   [21] De Lorenzo G, Fragiacomo P. Energy analysis of an SOFC system fed by syngas. Energy
647   Convers Manag 2015;93:175–86.
648

649   [22] Jia J, Abudula A, Wei L, Sun B, Shi Y. Thermodynamic modeling of an integrated
650   biomass gasification and solid oxide fuel cell system. Renew Energy 2015;81:400–10.
651

652   [23] Jia J, Abudula A, Wei L, Sun B, Shi Y. Effect of operating parameters on performance of
653   an integrated biomass gasifier, solid oxide fuel cells and micro gas turbine system.

35

654   Biomass and Bioenergy 2015;75:35–45.
655

656   [24]   Kartha S, Kreutz TG, Williams RH. Small-scale biomass fuel cell/gas turbine power
657   systems for rural areas. Energy Sustain Dev 2000;4:85–9.
658

659   [25]   Ghirardo F, Santin M, Traverso A, Massardo A. Heat recovery options for onboard fuel
660   cell systems. Int J Hydrogen Energy 2011;36:8134–42.
661

662   [26]   Piroonlerkgul P, Assabumrungrat S, Laosiripojana N, Adesina AA. Selection of
663   appropriate fuel processor for biogas-fuelled SOFC system. Chem Eng J 2008;140:341–
664   51.
665

666   [27]   Farhad S, Hamdullahpur F, Yoo Y. Performance evaluation of different configurations of
667   biogas-fuelled SOFC micro-CHP systems for residential applications. Int J Hydrogen
668   Energy 2010;35:3758–68.
669

670   [28]   Tjaden B, Gandiglio M, Lanzini A, Santarelli M, Järvinen M. Small-Scale Biogas-SOFC
671   Plant: Technical Analysis and Assessment of Different Fuel Reforming Options. Energy
672   & Fuels 2014;28:4216–32.
673

674   [29]   Santarelli M, Barra S, Sagnelli F, Zitella P. Biomass-to-electricity: Analysis and
675   optimization of the complete pathway steam explosion - enzymatic hydrolysis - anaerobic
676   digestion with ICE vs SOFC as biogas users. Bioresour Technol 2012;123:430–8.
677

678   [30]   Papurello D, Lanzini A, Tognana L, Silvestri S, Santarelli M. Waste to energy:
679   Exploitation of biogas from organic waste in a 500 Wel solid oxide fuel cell (SOFC)
680   stack. Energy 2015;85:145–58.
681

682   [31]   Trendewicz a. a., Braun RJ. Techno-economic analysis of solid oxide fuel cell-based
683   combined heat and power systems for biogas utilization at wastewater treatment facilities.
684   J Power Sources 2013;233:380–93.
685

686   [32]   Gandiglio M, Lanzini A, Santarelli M, Leone P. Design and Balance-of-Plant of a
687   Demonstration Plant With a Solid Oxide Fuel Cell Fed by Biogas From Waste-Water and
688   Exhaust Carbon Recycling for Algae Growth. J Fuel Cell Sci Technol 2014;11:031003.
689

690   [33]   Siefert NS, Litster S. Exergy & economic analysis of biogas fueled solid oxide fuel cell
691   systems. J Power Sources 2014;272:386–97.
692

693   [34]   Mehr AS, Mahmoudi SMS, Yari M, Chitsaz A. Thermodynamic and exergoeconomic
694   analysis of biogas fed solid oxide fuel cell power plants emphasizing on anode and
695   cathode recycling: A comparative study. Energy Convers Manag 2015;105:596–606.
696

697   [35]   Ranjbar F, Chitsaz A, Mahmoudi SMS, Khalilarya S, Rosen MA. Energy and exergy
698   assessments of a novel trigeneration system based on a solid oxide fuel cell. Energy
699   Convers Manag 2014;87:318–27.
700

701   [36]   Soltani S, Mahmoudi SMS, Yari M, Rosen MA. Thermodynamic analyses of an externally
702   fired gas turbine combined cycle integrated with a biomass gasification plant. Energy
703   Convers Manag 2013;70:107–15.
704

705   [37]   Al-Sulaiman FA, Dincer I, Hamdullahpur F. Energy analysis of a trigeneration plant based
706   on solid oxide fuel cell and organic Rankine cycle. Int J Hydrogen Energy 2010;35:5104–
707   13.
708

709   [38]   Landau L, Moran MJ, Shapiro HN, Boettner DD, Bailey M. Fundamentals of engineering
710   thermodynamics. John Wiley & Sons; 2010.
711

712   [39]   Gholamian E, Mahmoudi SMS, Zare V. Proposal, exergy analysis and optimization of a
713   new biomass-based cogeneration system. Appl Therm Eng 2016;93:223–35.
714

715   [40]   Zainal ZA, Ali R, Lean CH, Seetharamu KN. Prediction of performance of a downdraft
716   gasifier using equilibrium modeling for different biomass materials. Energy Convers
717   Manag 2001;42:1499–515.
718

719   [41]   Jayah TH, Aye L, Fuller RJ, Stewart DF. Computer simulation of a downdraft wood
720   gasifier for tea drying. Biomass and Bioenergy 2003;25:459–69.
721

722   [42]   Jarungthammachote S, Dutta A. Thermodynamic equilibrium model and second law
723   analysis of a downdraft waste gasifier. Energy 2007;32:1660–9.
724

725   [43]   Tao G, Armstrong T, Virkar A. Intermediate temperature solid oxide fuel cell (IT-SOFC)
726   research and development activities at MSRI. Ninet. Annu. ACERC&ICES Conf. Utah,
727   2005.
728

729   [44]   Buswell AM, Hatfield WD. Anaerobic fermentations. Bull 1936;32.
730

731   [45]   Wellinger A, Murphy JD, Baxter D. The biogas handbook: science, production and

applications. Elsevier; 2013.

[46]   Ryu C, Yang Y Bin, Khor A, Yates NE, Sharifi VN, Swithenbank J. Effect of fuel properties on biomass combustion: Part I. Experiments-fuel type, equivalence ratio and particle size. Fuel 2006;85:1039–46.

[47]   Chan SH, Ho HK, Tian Y. Modelling of simple hybrid solid oxide fuel cell and gas turbine power plant. J Power Sources 2002;109:111–20.

[48]   Bejan A, Moran MJ. Thermal design and optimization. John Wiley & Sons; 1996.

[49]   Ahmadi P, Dincer I, Rosen MA. Development and assessment of an integrated biomass-based multi-generation energy system. Energy 2013;56:155–66.

[50]   Tsatsaronis G, Lin L, Pisa J. Exergy costing in exergoeconomics. J Energy Resour Technol 1993;115:9–16.

[51]   Mehr AS, Zare V, Mahmoudi SMS. Standard GAX versus hybrid GAX absorption refrigeration cycle: From the view point of thermoeconomics. Energy Convers Manag 2013;76:68–82.

[52]   Wongchanapai S, Iwai H, Saito M, Yoshida H. Selection of suitable operating conditions for planar anode-supported direct-internal-reforming solid-oxide fuel cell. J Power Sources 2012;204:14–24.

[53]   Lanzini A, Santarelli M, Orsello G. Residential solid oxide fuel cell generator fuelled by ethanol: Cell, stack and systemmodelling with a preliminary experiment. Fuel Cells 2010;10:654–75.

[54]   Madi H, Lanzini A, Diethelm S, Papurello D, Van herle J, Lualdi M, et al. Solid oxide fuel cell anode degradation by the effect of siloxanes. J Power Sources 2015;279:460–71. doi:10.1016/j.jpowsour.2015.01.053.

[55]   Al-Sulaiman FA, Dincer I, Hamdullahpur F. Energy and exergy analyses of a biomass trigeneration system using an organic Rankine cycle. Energy 2012;45:975–85.

[56]   Farhad S, Yoo Y, Hamdullahpur F. Effects of fuel processing methods on industrial scale biogas-fuelled solid oxide fuel cell system for operating in wastewater treatment plants 2010;195:1446–53.

38

771

[57]   Bang-Møller C, Rokni M, Elmegaard B. Exergy analysis and optimization of a biomass gasification, solid oxide fuel cell and micro gas turbine hybrid system. Energy 2011;36:4740–52.

[58]   El-Emam RS, Dincer I, Naterer GF. Energy and exergy analyses of an integrated SOFC and coal gasification system. Int J Hydrogen Energy 2012;37:1689–97.

[59]   Wongchanapai S, Iwai H, Saito M, Yoshida H. Performance evaluation of an integrated small-scale SOFC-biomass gasification power generation system. J Power Sources 2012;216:314–22.

[60]   Campitelli G, Cordiner S, Gautam M, Mariani A, Mulone V. Biomass fueling of a SOFC by integrated gasifier: Study of the effect of operating conditions on system performance. Int J Hydrogen Energy 2013;38:320–7.

[61]   Arteaga-Pérez LE, Casas-Ledón Y, Pérez-Bermúdez R, Peralta LM, Dewulf J, Prins W. Energy and exergy analysis of a sugar cane bagasse gasifier integrated to a solid oxide fuel cell based on a quasi-equilibrium approach. Chem Eng J 2013;228:1121–32.

[62]   Morandin M, Maréchal F, Giacomini S. Synthesis and thermo-economic design optimization of wood-gasifier-SOFC systems for small scale applications. Biomass and Bioenergy 2013;49:299–314.

[63]   Ozcan H, Dincer I. Performance evaluation of an SOFC based trigeneration system using various gaseous fuels from biomass gasification. Int J Hydrogen Energy 2014:1–10.

[64]   Caliandro P, Tock L, Ensinas A V., Marechal F. Thermo-economic optimization of a Solid Oxide Fuel Cell - Gas turbine system fuelled with gasified lignocellulosic biomass. Energy Convers Manag 2014;85:764–73.

[65]   Curletti F, Gandiglio M, Lanzini A, Santarelli M. Large size biogas-fed Solid Oxide Fuel Cell power plants with carbon dioxide management : Technical and economic optimization 2015;294.

[66]   Lv X, Liu X, Gu C, Weng Y. Determination of safe operation zone for an intermediate-temperature solid oxide fuel cell and gas turbine hybrid system. Energy 2016;99:91–102.

808

39

809

810   **Figures' caption**

811

812   Figure 1 schematic diagram of CHP system based on a) digester coupled SOFC, b) gasifier coupled
813   SOFC

814   Figure 2 Effect of current density on first and second law efficiencies of power generating system

815   Figure 3 Effect of current density on a) first and second law efficiencies of CHP system b) net power
816   output and heating value of CHP system

817   Figure 4 effect of current density unit product cost of heat and power

818   Figure 5 Effect of stack temperature difference on second law efficiency of power generating and CHP
819   system

820   Figure 6 effect of stack temperature difference on a) net power output and heating capacity b) unit
821   product cost of heating and power c) total product cost of digester coupled SOFC and gasifier coupled
822   SOFC

823   Figure 7 Comparison of a) first and second law efficiencies of systems as well as the total product cost
824   b) net output power and heating load of systems as well as the their product costs

825   Figure 8 Grassman diagram of the a) digester coupled CHP system based on SOFC (D-SOFC) b)
826   gasifier coupled CHP system based on SOFC (G-SOFC)

827

828

829

830

831

832

833

834

Tables' Caption

836   Table 1. Input data for the SOFC systems [34,37,45,55]
837   Table 2 Ultimate analysis of MSW [39]
838   Table 2. The comparison of the component percentages in the producer gas obtained from the gasification
839   in the present work and those reported in the literature, for wood with a moisture content of 16% and for a
840   gasification temperature of 1100K.
841   Table 3. Comparison of results obtained from the present work with the experimental values reported by
842   Tao et al. [43]
843   Table 4 Input data* and cost and auxiliary equations for each component [11,33]
844   Table 6. Exergy and exergy destruction rates for two proposed SOFC systems
845   Table 7 Exergoeconomic analysis results for the gasifier coupled SOFC
846   Table 8 Exergoeconomic analysis results for the Digester coupled SOFC
847   Table A.1. Material Resistivity used for ohmic voltage loss estimation [52]
848   Table A.2. Parameters correspond to anode and cathode sides material [52]
849

850

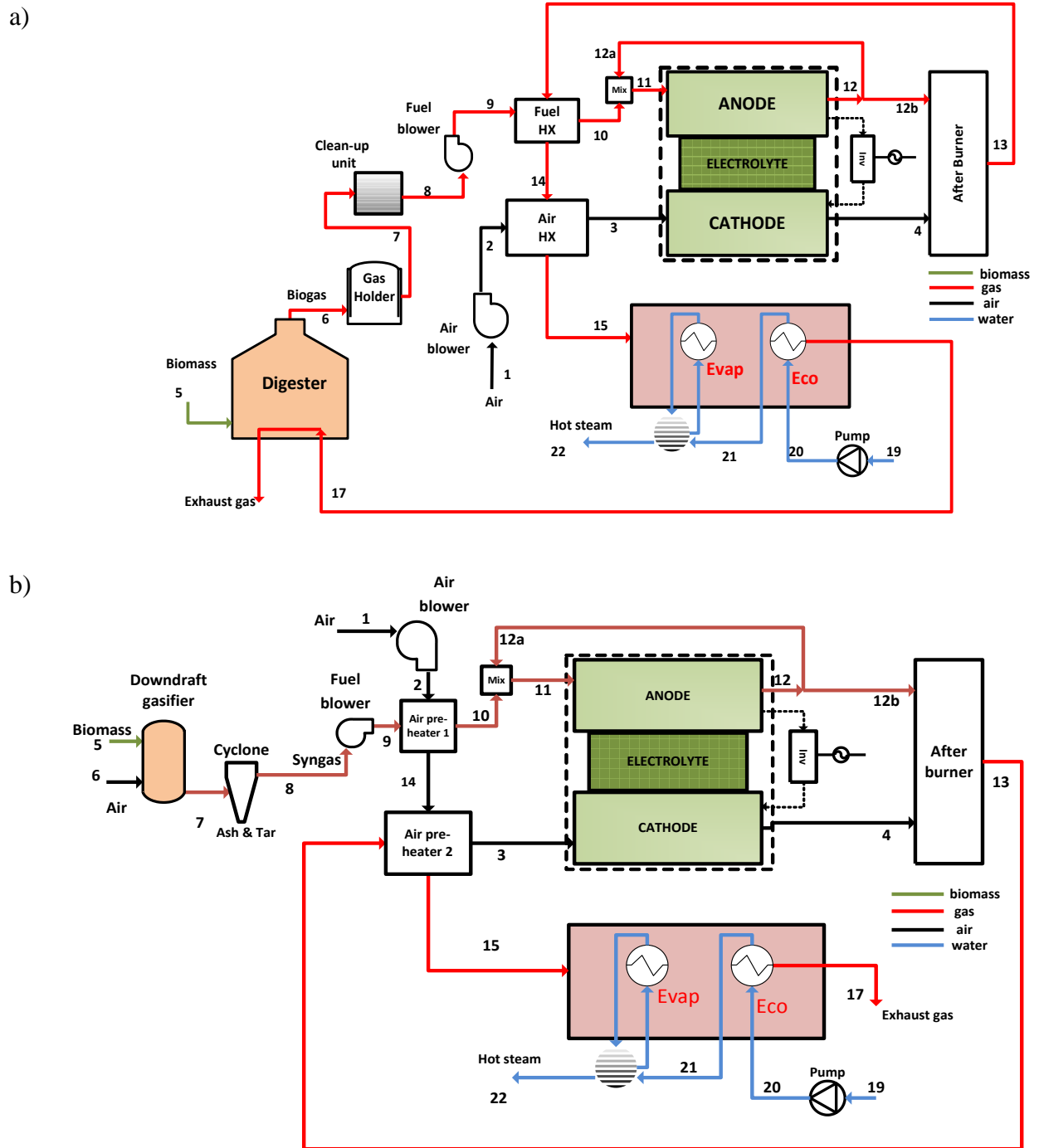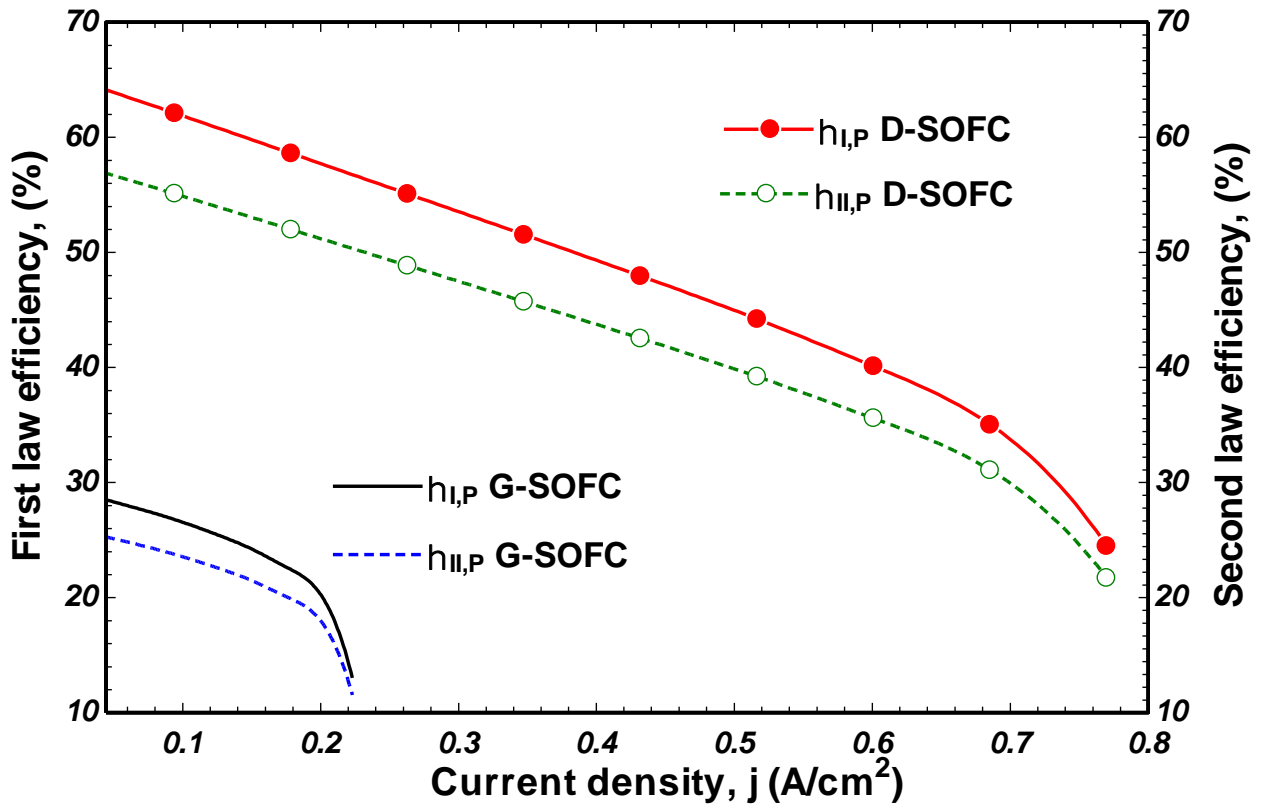851

852

853

854

855

856

857

858

Figures

a)

b)

Figure 1 schematic diagram of CHP system based on a) digester coupled SOFC, b) gasifier coupled SOFC
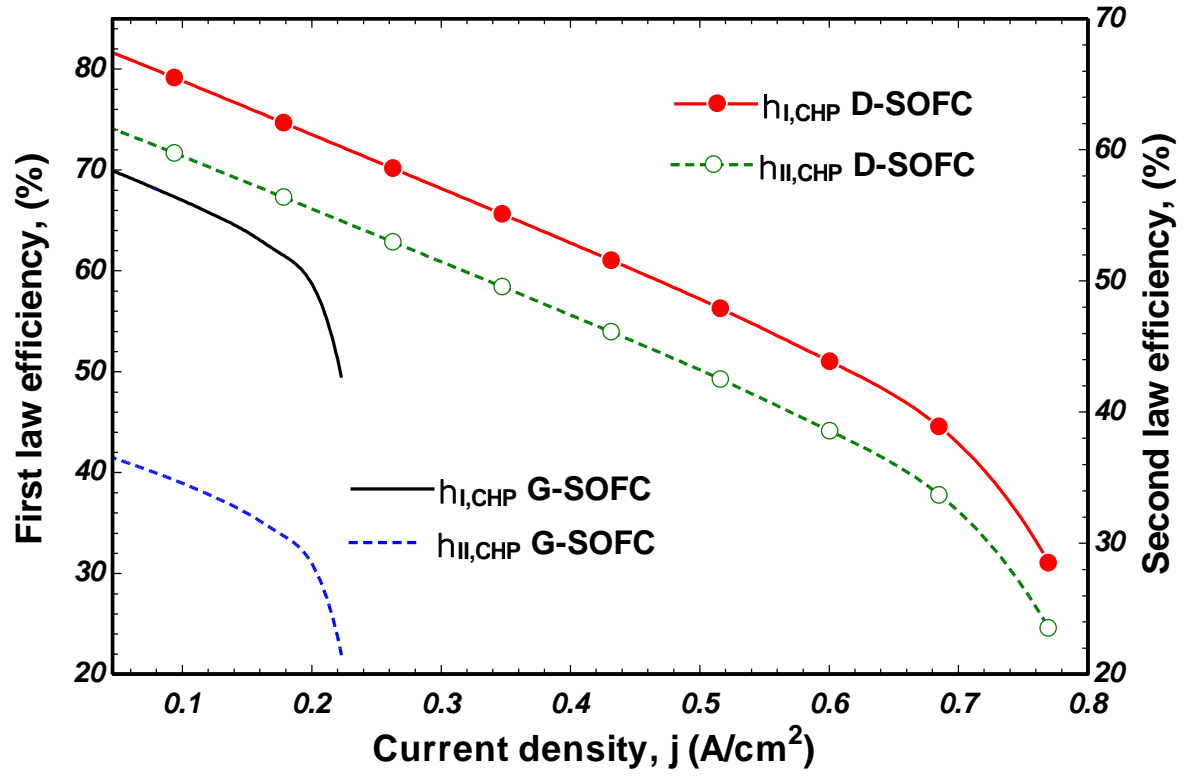
861

862

863

864

865

866

867

Figure 2 Effect of current density on first and second law efficiencies of power generating system

868

869

870

a)
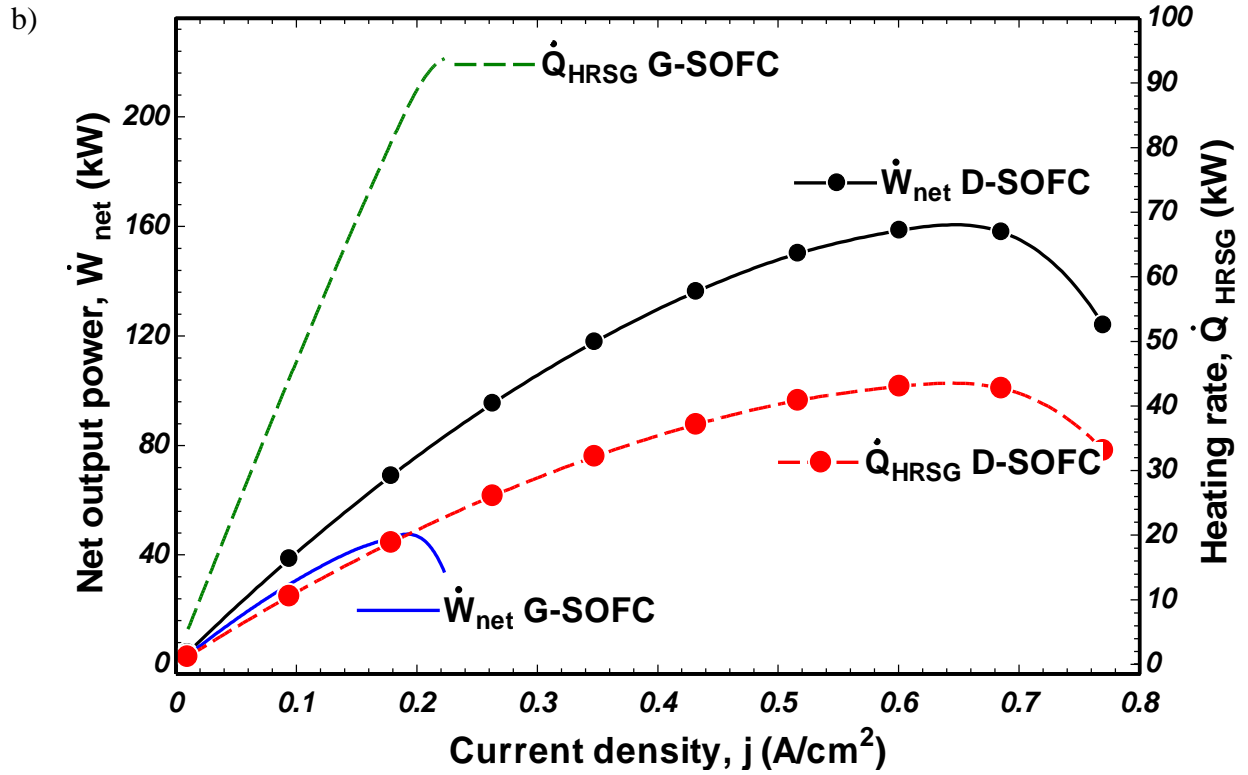
Figure 3 Effect of current density on a) first and second law efficiencies of CHP system b) net power output and heating value of CHP system

872

873

874

875

876

877

878

879

880

881

882

883

884
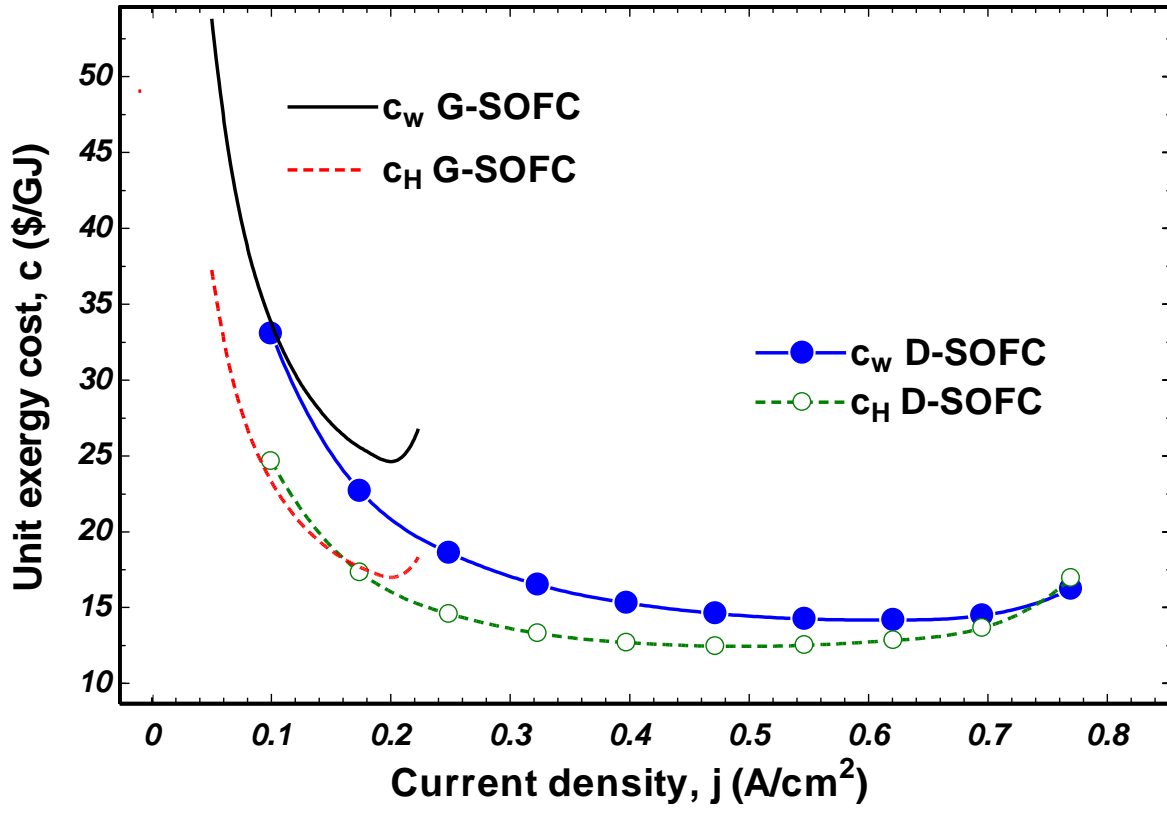
Figure 4 effect of current density unit product cost of heat and power

885

886

887

888

889

890
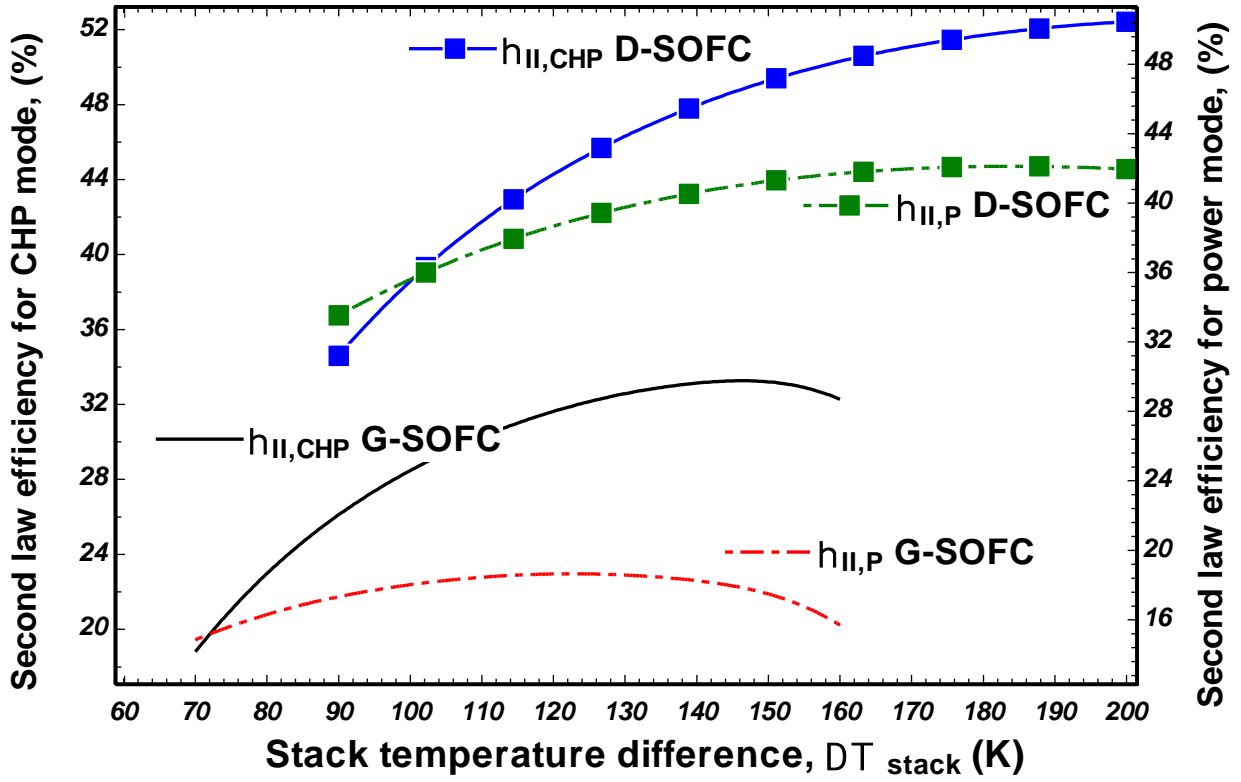
891

Figure 5 Effect of stack temperature difference on second law efficiency of power generating and CHP system

892
893

894

895

896

897

a)

b)

c)
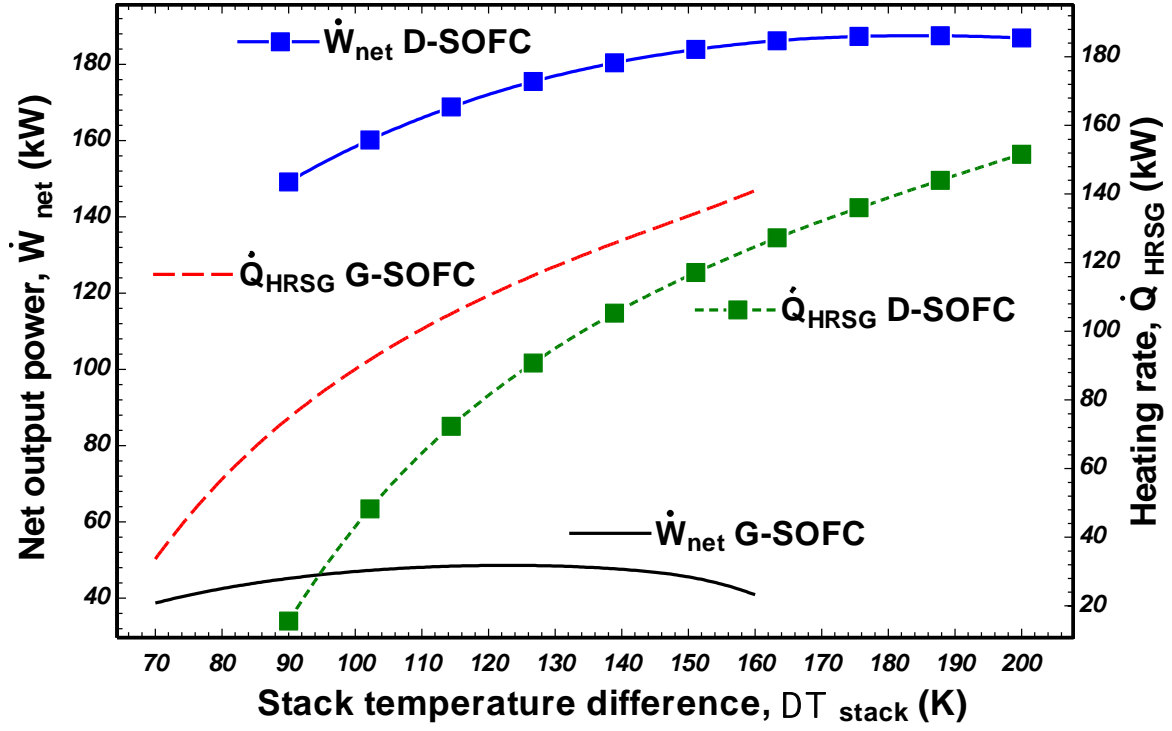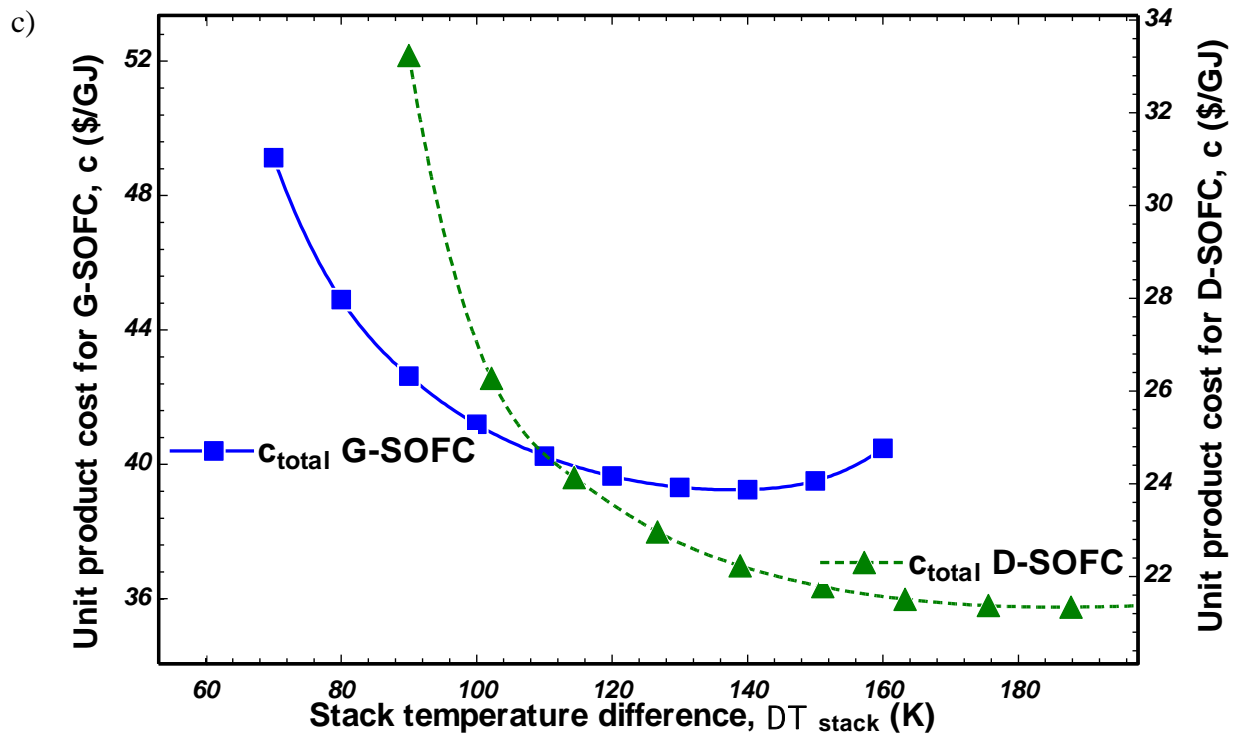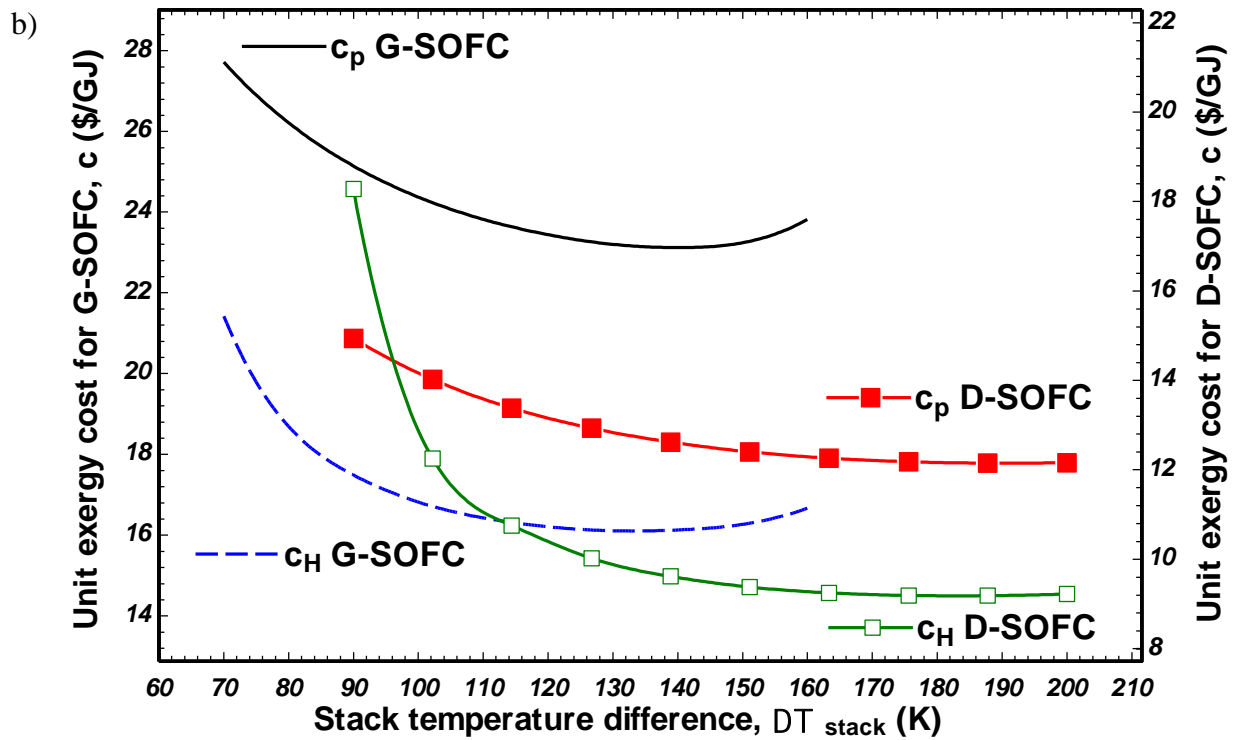
Figure 6 effect of stack temperature difference on a) net power output and heating capacity b) unit product cost of heating and power c) total product cost of digester coupled SOFC and gasifier coupled SOFC

a)

b)
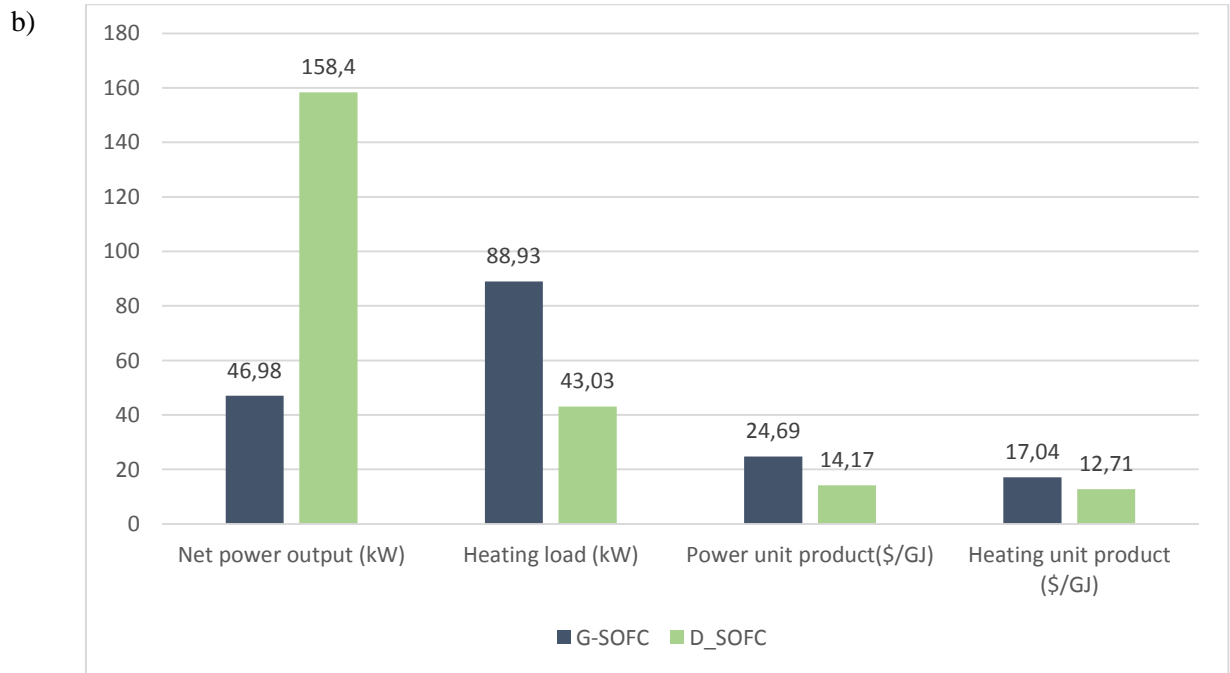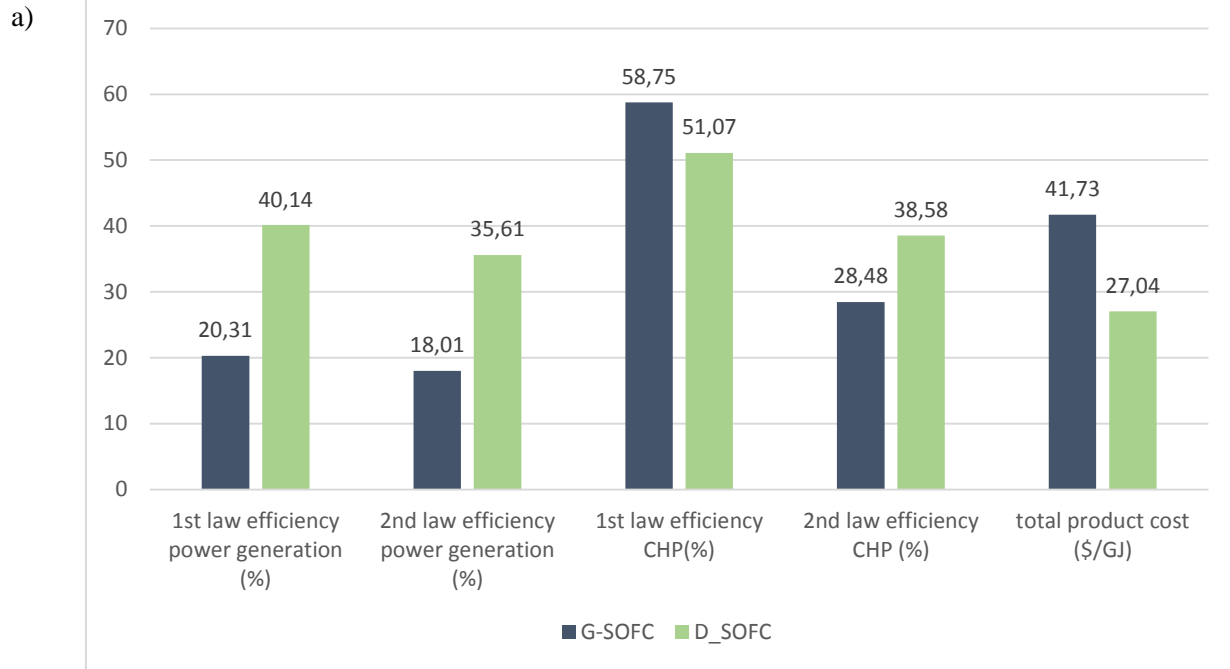
Figure 7 Comparison of a) first and second law efficiencies of systems as well as the total product cost b) net output power and heating load of systems as well as the their product costs

a)

17

$\dot{E}_{D,AB}$

After Burner

16   7

$\dot{W}_{stack}$

$\dot{E}_{D,stack}$

Inverter

14   Stack   5

13

Mix   4

15   Mix   6

$\dot{E}_{D,FHX}$

18   FHX   11

$\dot{W}_{AirB}$ 1 $\dot{E}_{Air}$

Air Blower

$\dot{E}_{D,AirB}$ 2

$\dot{E}_{D,FuelB}$

Fuel Blower   10   3   AHX

$\dot{W}_{FuelB}$

$\dot{E}_{D,Digester}$ 19 $\dot{E}_{D,AHX}$

21    $\dot{E}_{Exhaust}$ Pump

$\dot{E}_{D,HRSG}$ HRSG   22

Digester   9   20   23 $\dot{E}_{D,Pump}$

$\dot{E}_{Hot\ steam}$ $\dot{W}_{pump}$

8   24

$\dot{E}_{biomass}$
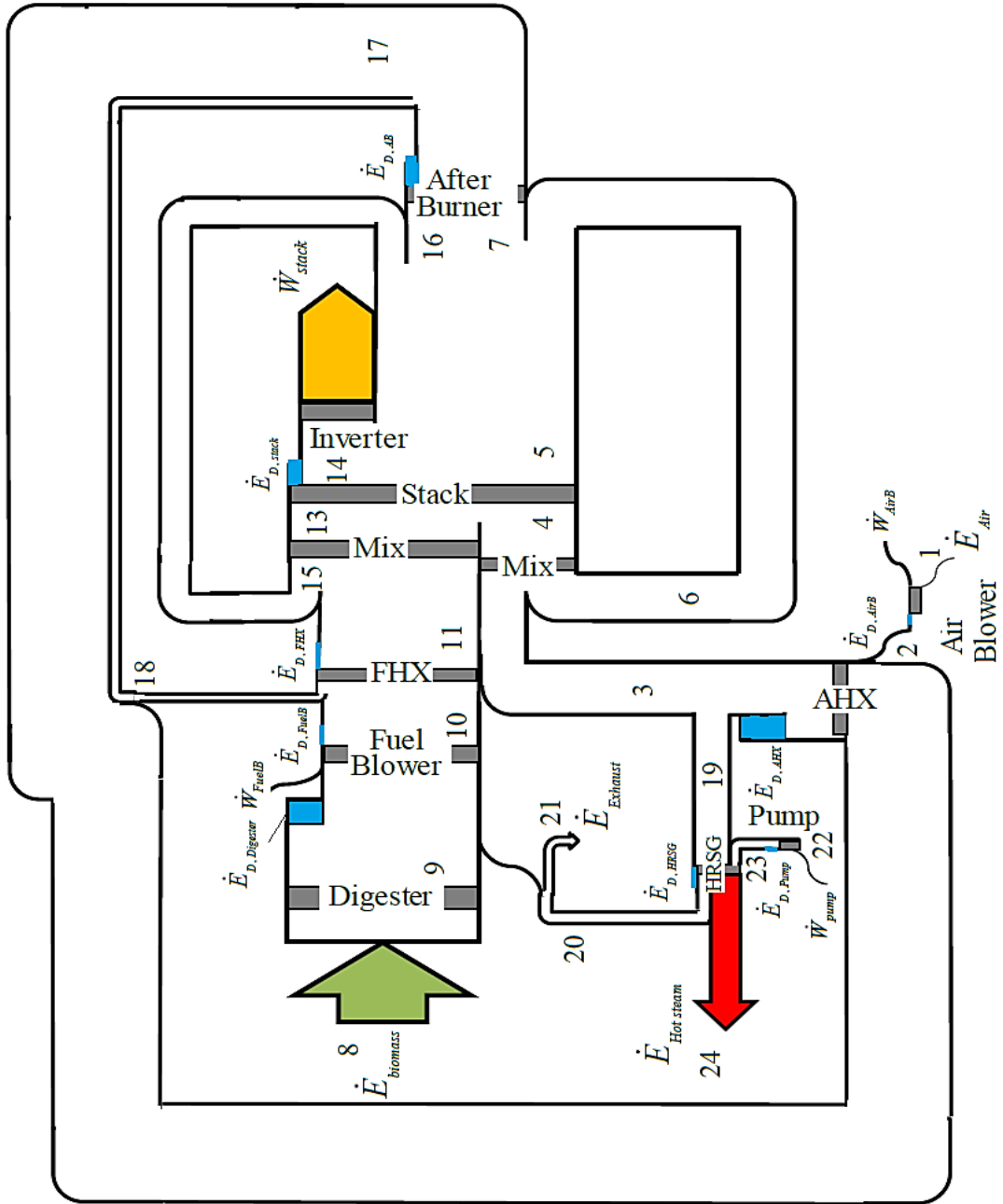
b)
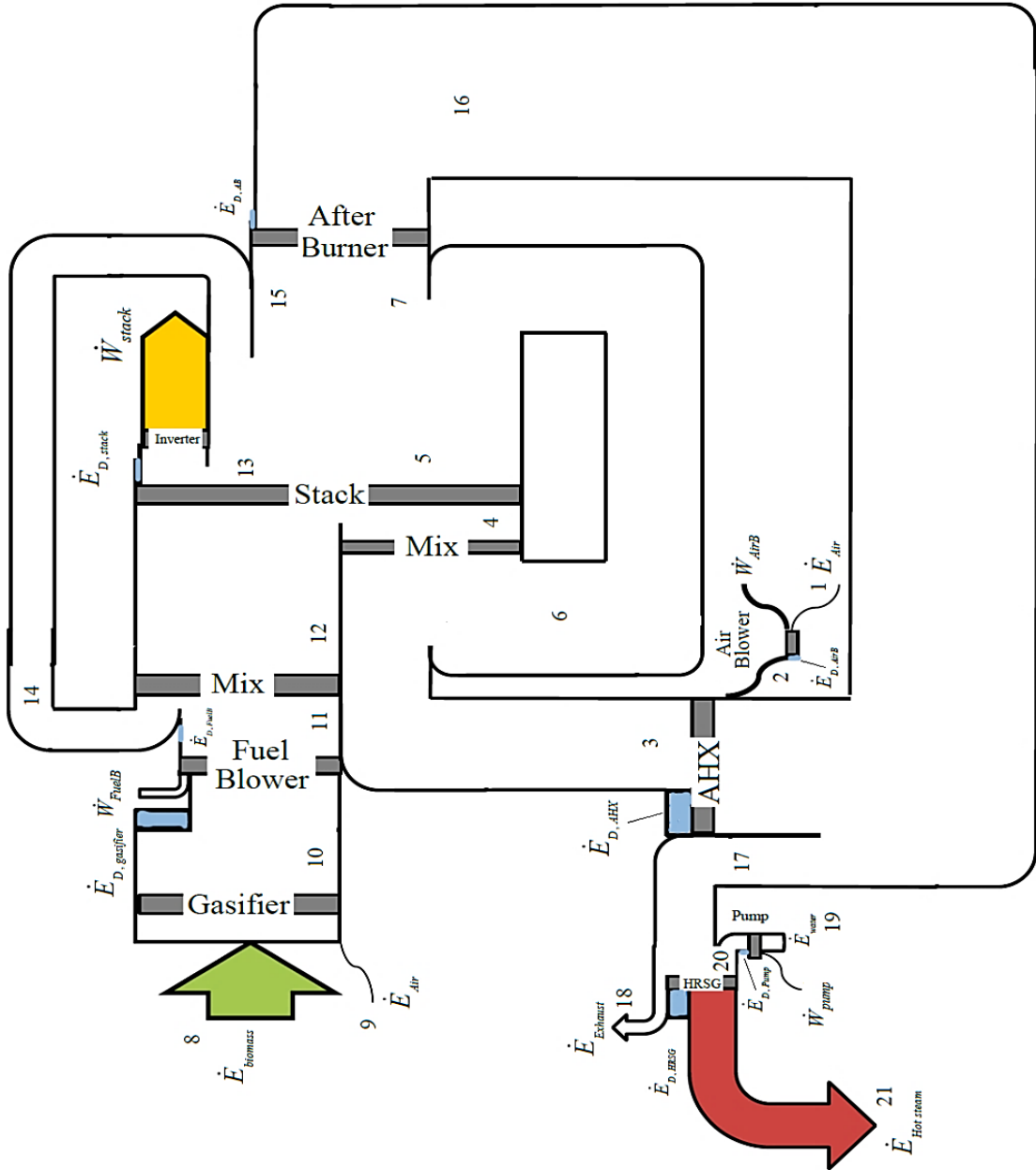
Figure 8 Grassman diagram of the a) digester coupled CHP system based on SOFC (D-SOFC) b) gasifier coupled CHP system based on SOFC (G-SOFC)

900

901

902

903   **Tables**

Table 1. Input data for the SOFC systems [34,37,45,55]

SOFC system			Unit
	Temperature difference between stack inlet and outlet	100	K
	Fuel utilization factor for whole SOFC	0.80	-
	Active surface area	50	cm^2
	DC-AC inverter efficiency	97	%
	Base inlet temperature to SOFC	973.15	K
	Steam to carbon ratio	2	-
	Thickness of anode	500	μm
	Thickness of cathode	50	μm
	Thickness of electrolyte	10	μm
	Fuel blower isentropic efficiency	80	%
	Air blower isentropic efficiency	80	%
	Pump isentropic efficiency	80	%
	Number of cells	11,000	-
	Afterburner combustion efficiency	99	%
	Stack pressure drop	2	%
	Heat exchangers pressure drop	3	%
	Afterburner pressure drop	5	%
Digester			
	Work needed to drive the fan	0	kW
	Exit temperature (Thermophilic digester)	328	K
	Amount of volatile solid	95	%
	Amount of destruction in digester	70	%
Gasifier			
	Gasification temperature	1073.15	K
	Heat loss from gasifier	0	%
	Air inlet temperature	298	K
	Biomass inlet temperature	298	K
HRSG			
	Pinch point temperature difference	15	K
	Steam pressure	10	bar
	Water pump isentropic efficiency	0.75	-

904

905

906

907

Table 2 Ultimate analysis of MSW [39]

Biomass	C	H	N	S	O	Ash	Higher heating value (kJ/kmol)
Municipal solid waste	47.6	6	1.2	0.3	32.9	12	433034

908

909

Table 3. The comparison of the component percentages in the producer gas obtained from the gasification in the present work and those reported in the literature, for wood with a moisture content of 16% and for a gasification temperature of 1100K.

Constituent	Present model	Experiment [40]	Jarungthammachote equilibrium model [42]
Hydrogen	17.15	15.5	18.04
Carbon monoxide	19.28	19.1	17.86
Methane	0.55	1.1	0.11
Carbon dioxide	10.81	11.4	11.84
Nitrogen	52.21	52.9	52.15

910

911

Table 4. Comparison of results obtained from the present work with the experimental values reported by Tao et al. [43]

Current density (A/m^2)	Cell voltage (V) (Present work)	Cell voltage (V) (Tao et al.)	Error (%)	Power density (W/m^2) (Present work)	Power density (W/m^2) (Tao et al.)	Error (%)
2000	0.742	0.76	-2.368	0.148	0.15	-1.333
3000	0.684	0.68	0.588	0.205	0.21	-2.381
4000	0.634	0.62	2.258	0.253	0.26	-2.692
5000	0.582	0.57	2.105	0.294	0.295	-0.339
6000	0.547	0.52	5.192	0.328	0.315	4.127

912

913

914

915

916

917

Table 5 Input data[*] and cost and auxiliary equations for each component [11,33]

Auxiliary equations	Cost equations	Component
$c_{biomass}=2$	$Z_{gasifier}=1600\left(\dot{m}_{drybiomass}\right)^{0.67}$	Gasifier
$c_{biomass}=2$	$Z_{Digester}=350000\left(\dfrac{\dot{V}\,T}{21000}\right)^{0.75}$	Digester
$\dot{C}_{14}/\dot{E}_{14}=\dot{C}_{33}/\dot{E}_{33}$ $\dot{C}_{5}/\dot{E}_{5}=\dot{C}_{33}/\dot{E}_{33}$	$Z_{SOFC}=A_a\,N_{FC}\left(2.96\,T_{FC,e}-1907\right)$	SOFC stack
-	$Z_{AB}=\dfrac{46.08\dot{m}_7}{\left(0.955-\left(P_{17}/P_7\right)\right)}\left(1+e^{(0.018T_{17}-26.4)}\right)$	Afterburner
$c_1=0$	$Z_{AC}=91562\left(\dot{W}_{AC}/455\right)^{0.67}$	Air compressor
$c_{10}=c_F$	$Z_{FC}=91562\left(\dot{W}_{FC}/455\right)^{0.67}$	Fuel compressor
$c_{20}=0$	$Z_{P1}=1785\,f_n\left(\dot{W}_P/1\right)^{0.71}$ $f_n=1+\left(0.2/\left(1-\eta_P\right)\right)$	Pump
$\dot{C}_{17}/\dot{E}_{17}=\dot{C}_{18}/\dot{E}_{18}$	$Z_{FHX}=130\left(A_{FHX}/0.093\right)^{0.78}$	FHX
$\dot{C}_{18}/\dot{E}_{18}=\dot{C}_{19}/\dot{E}_{19}$	$Z_{AHX}=390\left(A_{AHX}/0.093\right)^{0.78}$	AHX
$\dot{C}_{19}/\dot{E}_{19}=\dot{C}_{20}/\dot{E}_{20}$	$Z_{HRSG}=6570\left(\left(\dot{Q}_{eco}/\Delta T_{eco}\right)^{0.8}+\left(\dot{Q}_{eva}/\Delta T_{eva}\right)^{0.8}\right)+$ $21276\dot{m}_{steam}+1184.4\left(\dot{m}_{gas}\right)^{1.2}$	HRSG
-	$Z_{inv}=100000\left(\dot{W}_{SOFC,DC}/500\right)^{0.7}$	Inverter

[*] $i_r=0.12$, $n=20$ years, $\tau=8000h$,T=retention time in digester, $c_F=2$/GJ (biomass)$

918

919

920

921

922

923

924

Table 6. Exergy and exergy destruction rates for two proposed SOFC systems

Digester Coupled SOFC		Gasifier Coupled SOFC	
Exergy rate	$\dot{EX}(kW)$	Exergy rate	$\dot{EX}(kW)$
Input exergy	462.6	Input exergy	290.3
Destruction		Destruction	
Digester	41.98	Gasifier	74.42
Air blower	7.018	Air blower	3.591
Fuel blower	0.128	Fuel blower	0.3248
AHX	78.67	AHX1	16.29
FHX	4.716	AHX2	35.3
Stack	42.29	Stack	9.304
AB	30.67	AB	12.95
Mixing unit	2.804	Mixing unit	1.018
HRSG	4.840	HRSG	9.786
Pump	0.049	Pump	0.010
Exergy associated with heating	26.27	Exergy associated with heating	54.29
Exergy associated with power	164.3	Exergy associated with power	49.81
Exergy loss	58.7	Exergy loss	26.93
U_f=0.80 , $Tstack = 800\ °C$			

925

926

927

928

929

930

931

Table 7 Exergoeconomic analysis results for the gasifier coupled SOFC (G-SOFC)

Components	$\dot{E}_f$ (kW)	$c_{F,k}$ ($/GJ)	$c_{P,k}$ ($/GJ)	$\dot{C}_{D,k}$ ($/h)	$\dot{C}_{L,k}$ ($/h)	$\dot{Z}_k$ ($/h)	$\dot{C}_{D,k}+\dot{C}_{L,k}+\dot{Z}_k$ ($/h)	f_k (%)
SOFC stack	437	16.8	20.05	0.5627	0	4.430	5.00	88.75
Air heat exchanger 1	15.36	4.751	27.87	0.2142	0	0.022	0.236	9.41
Air heat exchanger2	221.9	21.14	26.52	2.974	0	0.567	3.541	16.02
Air blower	15.62	20.05	34.01	0.2592	0	0.345	0.604	57.15
Fuel blower	6.25	20.05	29.92	0.0234	0	0.187	0.210	88.87
After burner	298.8	20.05	21.14	0.9345	0	0.191	1.126	16.99
Gasifier	260.8	2	3.968	0.5358	0	0.839	1.375	61.04
HRSG	37.06	21.14	33.84	0.7448	2.05	0.502	3.296	15.23
pump	0.0405	20.05	67.06	0.0007	0	0.004	0.005	85.78

U_f=0.80 , $Tstack = 800\ °C$

932

933

Table 8 Exergoeconomic analysis results for the digester coupled SOFC (D-SOFC)

Components	$\dot{E}_f$ (kW)	$c_{F,k}$ ($/GJ)	$c_{P,k}$ ($/GJ)	$\dot{C}_{D,k}$ ($/h)	$\dot{C}_{L,k}$ ($/h)	$\dot{Z}_k$ ($/h)	$\dot{C}_{D,k}+\dot{C}_{L,k}+\dot{Z}_k$ ($/h)	f_k (%)
SOFC stack	911.8	9.172	11.04	1.397	0	5.834	5.846	76.06
Air heat exchanger	441.8	11.87	15.28	3.361	0	1.130	4.452	24.51
fuel heat exchanger	12.81	11.87	19.44	0.2015	0	0.058	0.220	8.732
Air blower	30.53	11.04	20.73	0.2788	0	0.541	0.820	66.01
Fuel blower	0.753	11.04	33.46	0.0051	0	0.045	0.050	89.88
After burner	561.5	11.04	11.87	1.219	0	0.370	1.589	23.31
digester	444.4	2	2.277	0.3039	0	0.097	0.401	24.22
HRSG	18.04	11.87	25.23	0.2068	2.50	0.428	3.143	13.62
pump	0.014	11.04	64.49	0.0001	0	0.002	0.002	93.11

U_f=0.80 , $Tstack = 800\ °C$

934

935

936

937

Table 9. Comparison of the published works results with those of the present work

Research	Plant Type; Plant Scale	Fuel; Process; Gas	Thermodynamic analysis		Economic analysis	Year
			1st law Efficiency (%)	2nd law Efficiency (%)	Unit Product Cost	
Omosun et al. [14]	Cogeneration (Heat and power);200kW$_{el}$	Biomass; Fluidized bed gasification; Syngas (17%H$_2$,13%CO,11% CO$_2$,4%CH$_4$, 15%H$_2$O,40%N$_2$)	Electrical: 22.6% Total: 59.6%	-	2.9k £/kW$_e$ 1.1k £/kW$_T$	2004
Piroonlerkgul et al. [26]	Mono generation (power); small size (50-60kW)	Biogas (60%CH$_4$,40%CO$_2$)	Electrical: 59%	-	-	2008
Farhad et al. [56]	Cogeneration (Heat and power);small size (~1kW$_{el}$)	Biogas (60.8%CH$_4$,34.8%CO$_2$, 2.4%N$_2$,1.2%O$_2$,0.01% water)	Electrical: 22.6% Total: 59.6%	-	-	2010
Bang-Møller et al. [57]	Cogeneration (Heat and power) Hybrid system; medium size (~300kW)	Wood; two-stage gasification; syngas	Electrical: 58.2% Total: 87.5%	Electrical: 50.4% Total: 53.4%	-	2011
Santarelli et al. [29]	Cogeneration (Heat and power); medium size (scale–up 250kW)	Wheat straw; Two-stage anaerobic digester; biogas (55%CH$_4$,10%H$_2$,35% CO$_2$)	Electrical: 49.2% Total: 75.1%	-	-	2012
El-Emam et al. [58]	Mono generation (power) Hybrid system; Large size (~30MW)	Coal gasification; syngas(10.6%CO$_2$,51.6 %CO,0.1%CH$_4$,35.1% H$_2$,2.6%N$_2$)	Electrical: 38.1%	Electrical: 27%	-	2012
Wongchanapai et al. [59]	Mono generation (power); small scale (5kW)	Wood; two-stage gasification; Syngas(18.7%H$_2$,21.87 CO,0.22%CH$_4$,10.51% CO$_2$,47.3%N$_2$)	Electrical: 38.9%	Electrical: 37.4%	-	2012
Campitelli et al. [60]	Mono generation (power); small scale (1-2 kW)	Wood; autothermal gasification; syngas (17.8%H$_2$,9.4%CO,14 %CO$_2$,19.8%H$_2$O,0.1% CH$_4$)	Electrical: 24.7%	-	-	2013
Arteaga-Pérez et	Cogeneration	Sugar cane/rice husk;	Total:	Total:	-	2013

Reference	Application	Fuel; technology; syngas	Efficiency	Efficiency	Cost	Year
al. [61]	(Heat and power); medium size (456.5kW)	bubbling fluidized bed gasification; syngas (17.5%H_2O,40.1%N_2,0.6%O_2,6.5%CH_4,13.6%CO,12.4%CO_2,9.3%H_2)	55.48%	32.01%		
Morandin et al. [62]	Cogeneration (Heat and power) Hybrid system; small size (~40kW)	Wood; fluidized bed gasifier/Viking gasifier; syngas	Total:63% (For Viking gasifier case) / Total: 58% (For fluidized bed gasifier)	-	15000$/kW (For Viking gasifier case) / 8000 $/kW (For fluidized bed gasifier)	2013
Trendewicz and Braun [31]	Cogeneration (Heat and power); small, medium and large sizes (330kW,1530kW,6140kW)	Waste water; anaerobic digestion; biogas (56.6%CH_4,36.7%CO_2,5.8%H_2O)	Electrical: 51.6% / Total: 87.5%	-	3584 $/kW (large size) / 3916 $/kW (medium size) / 5780 $/kW (small size)	2013
Gandiglio et al.[28]	Trigeneration (Heat, power and Algae production); small scale (2kW$_{el}$)	Waste water; anaerobic digester; biogas (60%CH_4,40%CO_2)	Electrical: 52.56% / Total: 85.93%	-	-	2014
Siefert and Litster [33]	Mono generation (power)	Waste water; anerobic digestion; Biogas (45%CH_4,40%CO_2,15%H_2O)	-	Electrical: 58%	3610 $/kW	2014
Ozcan and Dincer [63]	Trigeneration (Heat. power and cooling); medium size (145.5kW)	ThermoChembubling fluidized bed gasifier; syngas (43.3%H_2,9.2%CO,28%CO_2,5.6% H_2O,4.7%CH_4)	Electrical: 42.2% / Total: 78.8%	Electrical: 36.5% / Total: 50.6%	-	2014
Caliandro et al. [64]	Mono generation (power) Hybrid system; small and medium sizes (103kW and 8000kW)	Wood; fast internally circulating fluidized bed gasifier/circulating fluidized bed gasifier/Viking gasifier; syngas	Electrical: 71% (circulating fluidized bed) / Electrical: 68.7% (Viking gasifier)	-	0.3 $/kWh (circulating fluidized bed-medium size) / 1.1$/kWh (Viking gasifier-small size)	2014
Jia et al. [22]	Cogeneration (Heat and	Wood; downdraft gasifier; syngas	Electrical: 42.94%	-	-	2015

	power) Hybrid system; small size (~40kW)		Total: 67.59%			
Curletti et al. [65]	Mono generation (power); large size (1MW$_{el}$)	Waste water; anaerobic digestion; biogas	Electrical: 58.85%	-	2.75 M$ Net present value	2015
Mehr et al. [34]	Mono generation (power); medium size (~400kW)	Biogas (50-70%CH_4,30%-50%CO_2)	Electrical: 46.09%	Electrical:43.92%	19.53 $/GJ	2015
Lv et al. [66]	Mono generation (power) Hybrid system; small size (182kW)	Wood; gasification; syngas(4.53%CH_4,23.64%H_2,13.87%CO,17.92%CO_2,40.04%N_2)	Electrical: 60.78%	-	-	2016
Present work	Cogeneration (Heat and power); small size	Municipal solid waste; downdraft gasifier; Syngas	Electrical: 20.31% Total: 58.75%	Electrical: 18.01% Total: 28.48%	24.69$/GJ	-
		Municipal solid waste ;anaerobic digestion; biogas	Electrical: 40.14% Total: 51.07%	Electrical:35.61% Total: 38.58%	14.17$/GJ	-

940

941

942

943

944

945

946

Table A.1. Material Resistivity used for ohmic voltage loss estimation [52]

Component	Material	Resistivity	Thickness (mm)
Anode	Ni/YSZ cermet	$\rho_{an}=2.98\times10^{-5}\exp(\frac{-1392}{T_{FC,e}})$	0.5
Cathode	LSM-YSZ	$\rho_{cat}=8.114\exp(\frac{600}{T_{FC,e}})$	0.05
Electrolyte	YSZ	$\rho_{ely}=2.94\times10^{-5}\exp(\frac{10350}{T_{FC,e}})$	0.01
Interconnection	Doped LaCrO3	0.0003215	-

947

948

949

Table A.2. Parameters correspond to anode and cathode sides material [52]

Component	Parameter	Value	Unit
Anode	Pre-exponential factor for anode, γ_{an}	6.54×10^{11}	A/m^2
	Activation energy for anode, $E_{a,an}$	140,000	J/mol
Cathode	Pre-exponential factor for cathode, γ_{ca}	2.35×10^{11}	A/m^2
	Activation energy for cathode, $E_{a,cat}$	137,000	J/mol

950

951

952

953

954